Technical University of Denmark

DTU

D5.2 Numerical tools

Møhlenberg, Flemming; Christensen, Erik Damgaard

Publication date:
2015

Document Version
Publisher's PDF, also known as Version of record

Link back to DTU Orbit

Citation (APA):
Møhlenberg, F., & Christensen, E. D. (2015). D5.2 Numerical tools.

DTU Library
Technical Information Center of Denmark

MERMAID

mermaidproject.eu

Seventh Framework Programme
Theme [OCEAN.2011-1]
"Innovative Multi-purpose off-shore platforms: planning, design and operation"
Grant Agreement no.: 288710
Start date of project*: 01 Jan 2012 - Duration: 48 month*

Numerical tools

Deliverable: D5.2	
Nature of the Deliverable:	Report
Due date of the Deliverable:	Month 36
Actual Submission Date:	26-02-2015
Dissemination Level:	PU
Produced by:	Flemming Møhlenberg
Contributors:	Partners
Work Package Leader Responsible:	Ole Svenstrup Petersen
Reviewed by:	Erik Damgaard Christensen

Version	Date	Revised Pages	Description of Changes
1.0	June 2014	-	1st Draft released
1.1	February 2015	-	Final

Table of contents

1   Numerical tools for Multi-Use Platform planning and design

1.1   Introduction

Planning of offshore constructions is seldom standard-design and often involves site specific issues. This is especially true working with Multi Use Platform, where two or more different types of structures must be designed to interact and to utilise all possible synergies in their function. The planning and design of MUPS in MERMAID has therefore not only involved standard engineering methods, but also advanced numerical tools, that can enable a detailed understanding of the environment and the interactions between the MUP and the surrounding water environments.

The intention of this report is to summarise the advanced methods developed and used during MERMAID to support the planning and design of MUP's and form a guideline and inspiration to planners on how to meet the challenges that turns up during design of such structures.

2   Numerical tools for offshore renewable energy planning

2.1   Atmospheric models

2.1.1   The WRF model for mesoscale reanalysis WRF

The Weather, Research and Forecasting (WRF) Model (Skamarock et al., 2008) is a mesoscale numerical weather prediction system designed to serve both operational forecasting and atmospheric research needs. The WRF modeling system is in the public domain and is freely available for community use. It is designed to be a flexible, state-of-the-art atmospheric simulation system that is portable and efficient on available parallel computing platforms. The WRF model is used worldwide for a variety of applications, from real-time weather forecasting, regional climate modeling, to simulating small-scale thunderstorms.

Although designed primarily for weather forecasting applications, ease of use and quality has brought the WRF model to be the model of choice for power forecasting and downscaling in wind energy applications. This model has been used in many wind-related studies at DTU Wind Energy: wind shear in the North Sea (Pena and Hahmann, 2011) and over Denmark (Draxl et al., 2014), organized convection in the North Sea (Vincent et al., 2012), gravity waves (Larsén et al., 2012), extreme winds (Larsén et al, 2012), energy production models (Marinelli et al., 2014), forecasting icing effect on wind farm production (Davis et al., 2014), among others.

The meteorological data are produced using a mesoscale reanalysis method, which uses a numerical weather prediction model to fill space and time gaps among observations. The method thus obtains high-resolution temporal and spatial climate or climate change information from relatively coarse-resolution global general circulation models or reanalysis. The strength in using the models to fill the observation gaps is that the fields are dynamically consistent, and they are defined on a regular grid. Additionally, the models respond to local forcing that adds information beyond what can be represented by the observations.

The use of WRF for downscaling comes from the assumptions presented in Hahmann et al. (2010). The mesoscale model simulations were initialized using the output of global atmospheric reanalysis. These were also used to define the boundary conditions of the simulations and to produce analysis fields used in the nudging. In this manner we assume that the reanalysis fields provide an appropriate description of the regions large-scale and synoptic flows, whereas the mesoscale model is used to resolve smaller scales and processes not properly simulated in the reanalysis due to its limited spatial resolution (Hahmann et al., 2010; Hahmann et al., 2014).

The simulations used to generate wind time series for the MERMAID project utilize the Advanced Research WRF (ARW-WRF) Version 3.5.1 model released on 23 September 2013. The model is integrated on a grid with horizontal spacing of 30 km × 30 km (see Figure 1) covering all Europe and neighboring regions in northern Asia. In the vertical, the model was configured with 41 levels with model top at 50 hPa. The lowest 12 of these levels are within 1000m from the surface and the first level is located at approximately 14 m AGL. More details of the model configuration and the model parameterizations used in the simulations are in Table 1. The used settings are similar to those used for the production of the wind atlases for the NORSEWind project (Hahmann et al., 2012) and South Africa (WASA; Hahmann et al., 2014b).
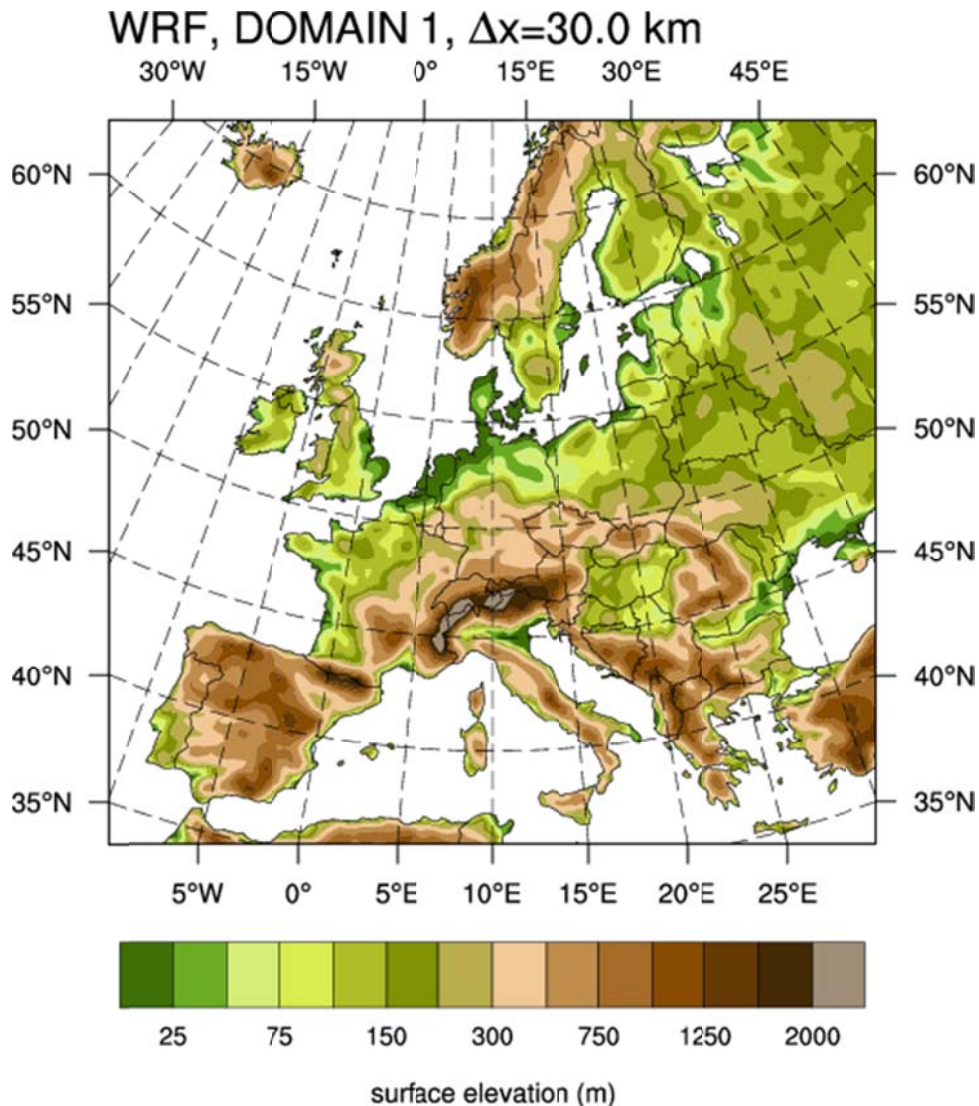
Figure 1. Domain extent and surface elevation (m) used in the WRF simulations.

In the simulation the ERA-Interim reanalysis (Dee et al., 2011) with 0.75°× 0.75° horizontal grid spacing was used to provide the large-scale weather conditions. The model sea surface temperatures (SST) came from a separate file (OISST; Reynolds et al. 2002) with increased horizontal resolution with respect to the reanalysis at $1/4° \times 1/4°$ grid spacing and daily time resolution. Higher resolution SST datasets exist, but they do not have the long temporal extent required. The control simulation covered the period 2000–2013, and was run in a series of 11-day long overlapping simulations, with the output from the first day being discarded. This method is based on the assumptions described in Hahmann et al. (2014). The simulation used grid nudging that continuously relaxes the model solution towards the gridded reanalysis (every 6 h) but this was done only on the outer domain and above the boundary layer (level 10, located ∼800 m AGL) to allow for the mesoscale processes near the surface to develop freely. Because the simulations were re-initialized every 10 days, the runs are independent of each other and can be integrated in parallel reducing the total time needed to complete a multi-year climatology. The grid nudging and frequent re-initialization keeps the model solution from drifting from the observed large-scale atmospheric

patterns, whereas the relatively long simulations guarantee that the mesoscale flow is fully in equilibrium with the mesoscale characteristic of the terrain.

The wind climatology produced from winds simulated by the WRF model in this analysis mode was verified against high-quality tall mast and wind LiDAR measurements over the North and Baltic Seas. At most offshore sites where measurements are not contaminated from the presence of a wind farm or nearby coastlines, errors in mean annual wind speed are under 0.35 m s−1 or 3.2% at heights 65 – 106 m. While the biases in annual mean wind speed are small, the WRF-derived wind climatologies exhibit reduced variability as compared to observations. The relative biases in the WRF wind speeds are lower than those that will be obtained from using wind fields directly from the atmospheric reanalysis and quantify the added value of the WRF model downscaling for ocean applications.

Model setup	ARW-WRF Version 3.5.1, released 23 September 2013.
	Mother domain (D1; 115 × 108 grid points) with 30 km grid spacing.
	Polar stereographic projection centered at 52.2°N, 10.0°E (Figure 1).
	41 vertical levels with model top at 50 hPa; 9 of these levels are placed within 1000 m of the surface; the first 6 levels are located at: 14, 43, 72, 100, 129 and 190 m AGL.
	MODIS land-cover classification (20 classes) of the International Geosphere-Biosphere Programme.
Simulation setup	Initial, boundary conditions and fields for grid nudging come from the ERA-Interim reanalysis on pressure levels and 0.75°× 0.75° resolution.
	Runs are started (cold start) at 00:00 UTC every 10 days and integrated for 11 days, the first 24 h of each simulation are discarded.
	Optimal interpolation SST (OISST; at 1/4°× 1/4° resolution and are updated daily. Sea-ice from this dataset also used with possible sea-ice fraction.
	Hourly model output for the lowest 11 levels.
	Time step 180 s.
	5-grid point boundary nudging zone.
	Grid nudging above level 10 for wind, temperature and water mixing ratio; nudging coefficient 0.0003 s^{-1}.
Model physics	Thompson Graupel scheme (option 8), Kain-Fritsch cumulus parametrization (option 1).
	RRTM scheme for longwave (option 1); Dudhia scheme for shortwave (option 1), activated every 30 minutes.
	Mellor-Yamada-Janjic scheme (Mellor and Yamada, 1982) (option 2), Eta similarity (option 2) surface layer scheme, Noah Land Surface Model (option 2).
	Simple diffusion (option 1); 2D deformation (option 4); 6th order positive definite numerical diffusion (option 2); no vertical damping.
	Positive definite advection of moisture and scalars.

Data post-processing	Wind speed log interpolated from adjacent model levels, log interpolation to zero wind at roughness length below model first level.
	For time series, horizontal interpolation from the four model vertices surrounding the desired coordinates.

The long-term mean wind speed simulated by the WRF model in the mesoscale analysis mode is presented in Figure 2. This is the same simulation used to extract wind time series used in the project. Examples of the wind climate at the four MERMAID offshore test study sites are presented in Figure 3.
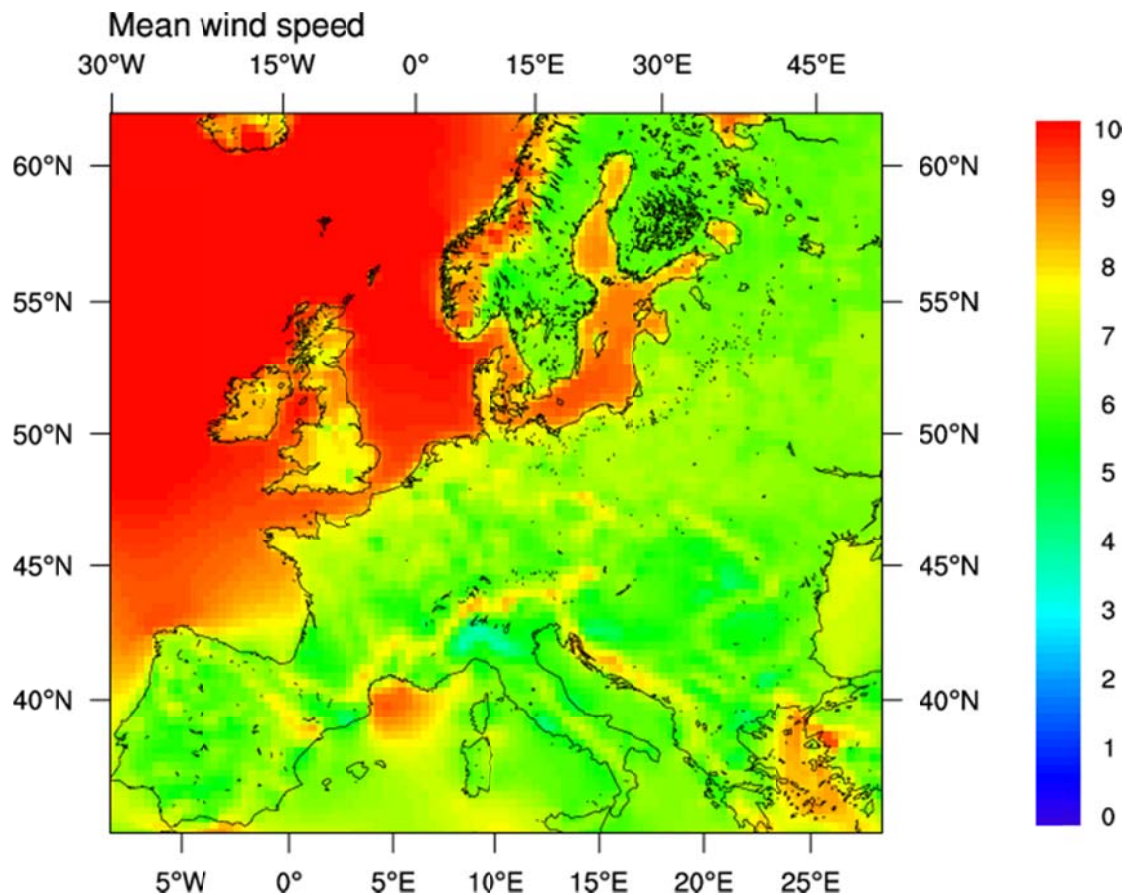
Figure 2. Long-term mean (2000−2013) wind speed (m s-1) simulated by the WRF model using the mesoscale analysis mode. The winds correspond to a height of 100 m AGL.

h= 100 m, 53.75 N 6.43 E
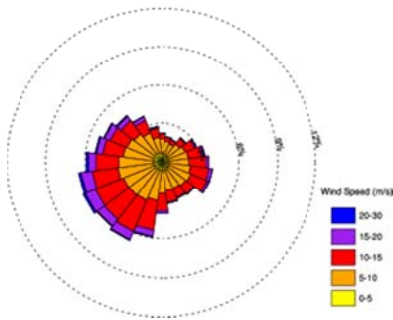
h= 100 m, 55.07 N 13.15 E
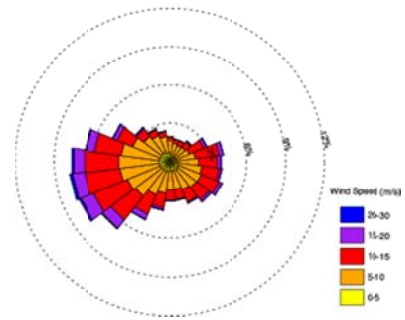
Southern North Sea site
Mean wind speed: 9.2 ms-1

Baltic site
Mean wind speed: 9.1 ms-1

h= 100 m, 43.39 N 4.13 W

h= 100 m, 45.24 N 12.40 E

Atlantic site
Mean wind speed: 5.8 ms-1

Mediterranean site
Mean wind speed: 5.5 ms-1

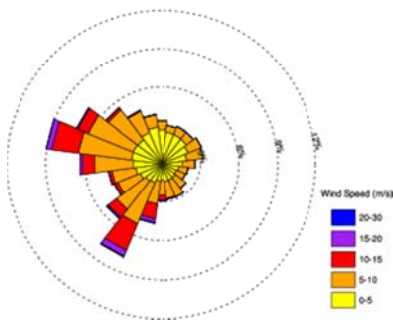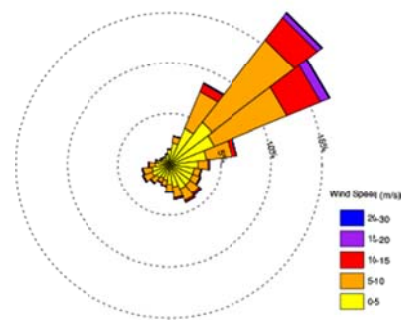*Figure 3 Examples of the wind climate at the four MERMAID offshore test study sites.*

2.2 Ocean wave models

2.3 Hydrodynamic models

2.3.1 Numerical tools for modelling wave attenuation caused by vegetation

Large scale offshore aquaculture in combination with offshore wind farms are studied for various sites in Europe. This is dealt with under EU-funded Framework Program 7 project called "MERMAID". As being a relatively new topic of research, the environmental impact of large scale aquaculture remains unknown. Such infrastructure can have a significant influence on the local hydrodynamics, i.e. waves, currents, turbulence energy, etc. Among those various environmental aspects, the impact of seaweed aquaculture on the local wave climate is explored in this study.

Depending on the local conditions, wave attenuation due to the presence of seaweed could generate adverse effects on the larger scale, influencing the transformation of adjacent coastlines as there is change in the local wave climate due to wave attenuation.

In terms of wave dissipation by aquatic vegetation, various studies have been conducted. The characteristics of vegetation, namely, surface area, vegetation length, mass density and stiffness have been studied concerning effect of wave attenuation (Augustin et al.). Besides, analyses with respect to effect of wave characteristics (Maza et al.), as well as combination with current on dissipation have been carried out by (Zhan Hu et al. 2014). Formulations representing the relevant processes like (Dalrymple et al., 1984 and extended by Mendez and Losada (2004)) are mainly based on laboratory tests and have subsequently been implemented in numerical tools to further study the effect of wave attenuations. After implementation of formulae in numerical wave model called SWAN, Tomohiro et al. (2011) concluded that this model has the ability to calculate two-dimensional wave dissipation over a vegetation field including some important aspects such as breaking and diffraction as used in SWAN model. However, all these researches merely considered vegetation which originates from the seabed. This situation is rather different from the seaweed aquaculture in which the seaweed is attached to floating structures, i.e. the seaweed only exists in the upper part. Therefore, more research is required to understand wave attenuation of floating seaweed.

Method
In order to determine the impact of floating seaweed on local waves, the numerical program called "SWAN" is applied. SWAN is a third-generation wave model which computes random, short-crested wind-generated waves in near shore region. It is developed at Delft University of Technology. In SWAN, various physical processes are accounted for: wave generation by wind, wave propagation in time and space, shoaling, refraction because of depth and current, triad and quadruplet interactions, white capping due to limit of wave steepness, depth-induced breaking, wave-induced set-up, transmission and reflection against obstacles, dissipation due to aquatic vegetation, turbulent flow and viscous fluid mud, and diffraction.

The most relevant physical process involved in this research is dissipation by aquatic vegetation. Other physical processes are irrelevant or can be neglected due to specific conditions of the offshore region. To be more specific, wind is not considered as we only take interest in wave attenuation effect caused by vegetation. The offshore region has relatively large water depth with a flat bed.

Consequently, shoaling, refraction, set-up, depth-induced breaking, bottom friction, etc. are omitted. In addition, and in order to focus on the effects of seaweed on wave propagation only, currents are not taken into consideration.

This computation of energy dissipation caused by underwater vegetation is based on the Dalrymple's formula (Dalrymple et al., 1984), in which the vegetation is schematised as cylinders and wave attenuation is realised by the work done by drag force on waves. Compared with this vegetation module, the seaweed aquaculture sees a remarkable difference. Unlike the vegetation implemented in the SWAN model starting from the bottom, the floating seaweed merely exists around the surface. As a result a modification is required to represent the floating seaweed in the real situations. This is achieved by implementing two vegetation layers vertically and applying a drag coefficient of zero to the lower layer, which is virtually existed.
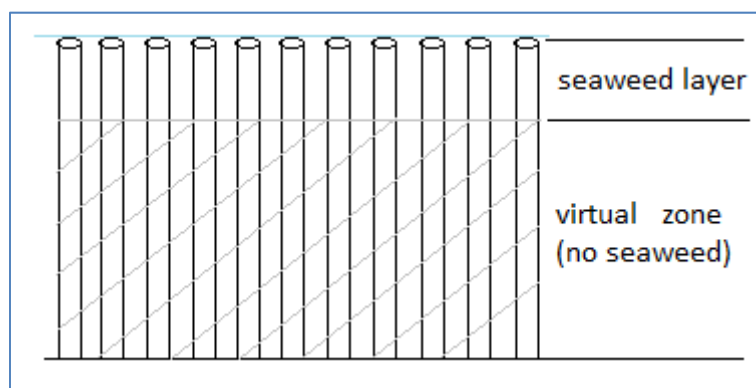
Figure 4   Vegetation schematisation in vertical direction

After setting up this model, sensitivity analysis has been carried out to determine individual impact of each parameter on the effect of wave attenuation. The sensitivity analysis follows the following configurations:
1. Impact of wave height on wave attenuation
2. Impact of wave period on wave attenuation
3. Impact of vegetation height on wave dissipation
4. Impact of vegetation diameter on wave dissipation
5. Impact of vegetation density on wave dissipation

In general, SWAN computations are able to be performed on a regular, curvilinear and a triangular mesh on a Cartesian or spherical coordinate system. In this study, a regular mesh, i.e. a rectangular computational area is properly used. An appropriate mesh size of 5 meter is chosen to resolve the relevant wave characteristics.

Input parameters are provided along the boundary of computational area. Wave height, wave period, wave incidence angle, boundary shape of spectrum in terms of irregular wave, such parameters are given in the command file. In the output command, we can prescribe SWAN to give outputs of several parameters such as wave height, wave direction, wave period, energy density along wave spectrum, etc. Two example results regarding change in wave height and wave height diagram for the whole computational area are described in the figures below. The first example represents the vegetation throughout the whole computational area and the second example

indicates a smaller patch in the middle of computational area, ranging from 45 m to 75 m in x axis and 40 m to 90 m in y axis. The patch is presented by the green area in figure 5.

Result example 1:
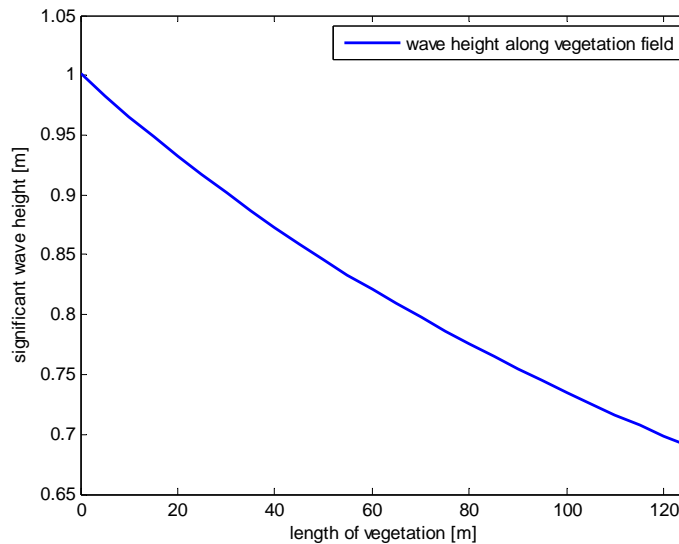
Figure 5   Wave height change for full vegetation

With an initial significant wave height of 1 meter (peak wave period 5 s, vegetation height 3 m, vegetation density 200 stems per square meter, drag coefficient 0.2), the wave height will reduce to somewhat lower than 0.7 meter after going through the applied vegetation field.
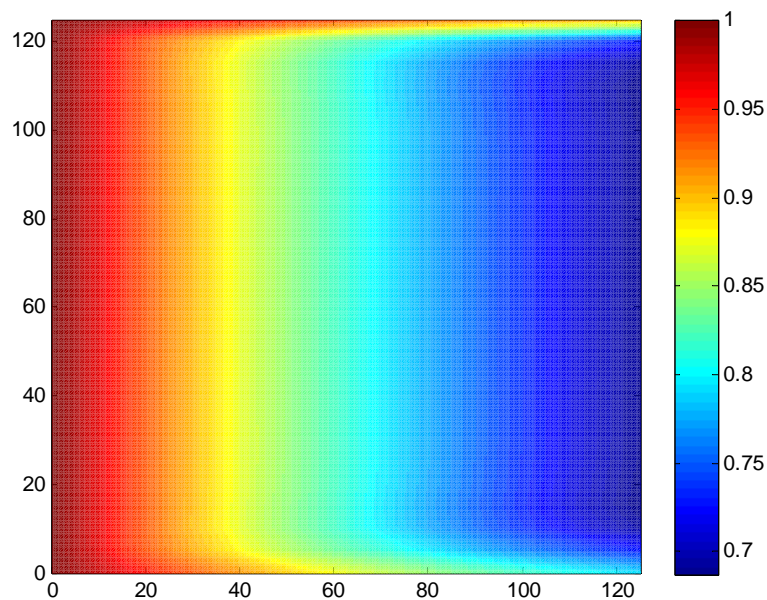
Figure 6 Wave height [m] field for the case with vegetation over the full extent of the model domain

Result example 2:
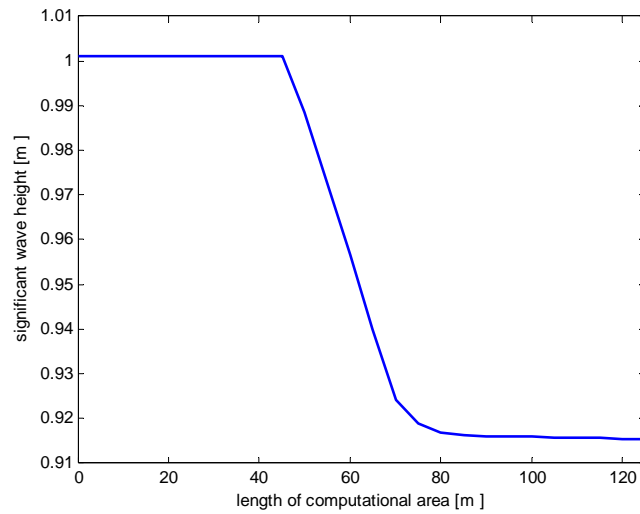
Figure 7 Wave height change for vegetation patch

Compared with Figure 5 in which the wave height decreases along the whole domain, the wave height in this figure only decreases in the middle range of computational area because the vegetation merely exists for that part. Moreover, the wave height reduces to approximately 0.9 meter, which is remarkably larger than that in example 1. This is reasonable as the wave goes through less vegetation field, so less attenuation is obtained.
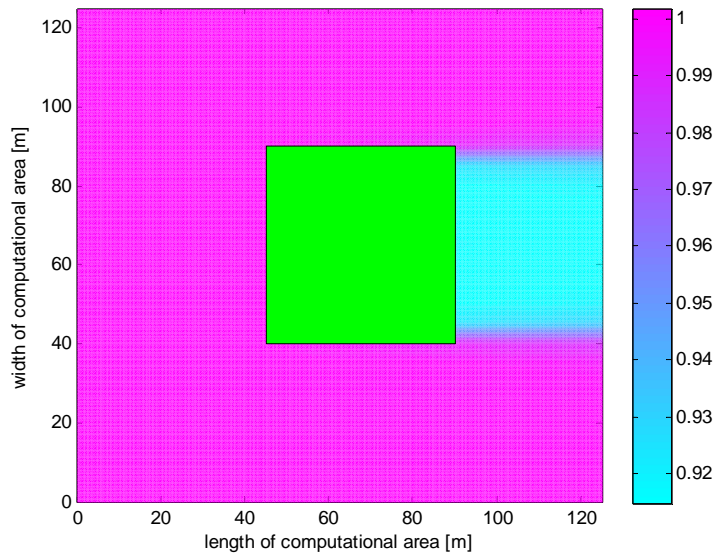
Figure 8   Wave height diagram for small vegetation patch

As can be easily seen from the two example results, at the leeside of the seaweed (from the propagation direction of the wave), the waves will be attenuated and therefore a change in the local wave climate will be the result.

The following steps in this study are to calibrate the model with experimental data from Technische Universität Braunschweig. After calibration and validation of the modeling approach, it will be applied to a case study in the North Sea.

2.4 Detailed flow models

2.4.1 CFD models (OpenFOAM)

Modelling the detailed flow around offshore structures such as wind turbine foundations, fish cages or moorings require a high spatial resolution and also solution of the full Navier-Stokes equations, normally using so-called Computational Fluid Dynamics (CFD) models. In the MERMAID one of the CFD models used extensively is the OpenFoam model.

The OpenFoam model was based on the open source CFD libraries OpenFoam® where the Navier-Stokes equations were solved based on a finite volume discretization on a collocated grid arrangement. The model was implemented on polyhedral meshes giving a large flexibility regarding unstructured meshes. Interpolation of the discretised equations in order to apply the Gauss theorem was achieved by first or higher order schemes. The iterative solution algorithm included multigrid methods which provide a fast convergence with a low number of iterations. (Jasak et al, 2007; Openfoam, 2014)

The Reynolds averaged Navier-Stokes equations needs a closure model, the so-called turbulence model. Several possibilities are applied for various applications. The Reynolds Averaged models include the standard k-epsilon and k-omega models where the latter has been applied for simulations involving wave and current boundary layers and sediments transport (Fuhrman et al, 2010). The Large Eddy Simulations (LES) models include the Smagorinsky model and the k-equation model which is an extension of the Smagorinsky model to include the transport of turbulent kinetic energy Villiers, 2006). This closure model has been applied for simulating the mixing process of saline stratifications around bridge piers where the resolution of large eddies is important to represent the correct mixing process. The mixing of different densities was achieved by assigning the properties such as densities of the different layers to scalar fields which were allowed to completely mix. From the mixture scalar field the properties of the mixed water were derived (Brennan, 2001).

For coastal and marine applications the model includes a free surface formulation by the Volume of Fluid (VOF) method Hirt et al, 1981; Rusche, 2002). Hereby it is possible to simulate free surface water waves and the interaction with coastal and marine structures. The model includes wave generation boundary conditions which allows for representation of regular waves as well as irregular sea states based on a given wave spectrum (Jacobsen et al, 2012). In this way investigations have been made on wave impact and run-up on wind turbine foundations, boat landings, and secondary structures (Bredmose et al, 2011; Paulsen et al, 2014). In order to represent coastal structures such as rubble mound breakwaters the model is extended to handle the flow in a porous media by means of the volume averaged Reynolds averaged Navier-Stokes equations (VARANS) (Jensen et al, 2014). With this model processes such as the reflection, transmission and overtopping can be simulated for e.g. caisson and rubble mound breakwaters while stability of sea walls and scour protection armor layers can be estimated (Jensen et al, 2014).

In the planning of MUP installations CFD can be used in a variety of cases. In Mermaid CFD has been applied to describe the flow and mixing induced by vertical monopiles in stratified currents (see Figure 9). The near-field dispersion of dredging spill from installation of gravity based wind turbine foundations or when installing scour protection armoring around foundations is another example.
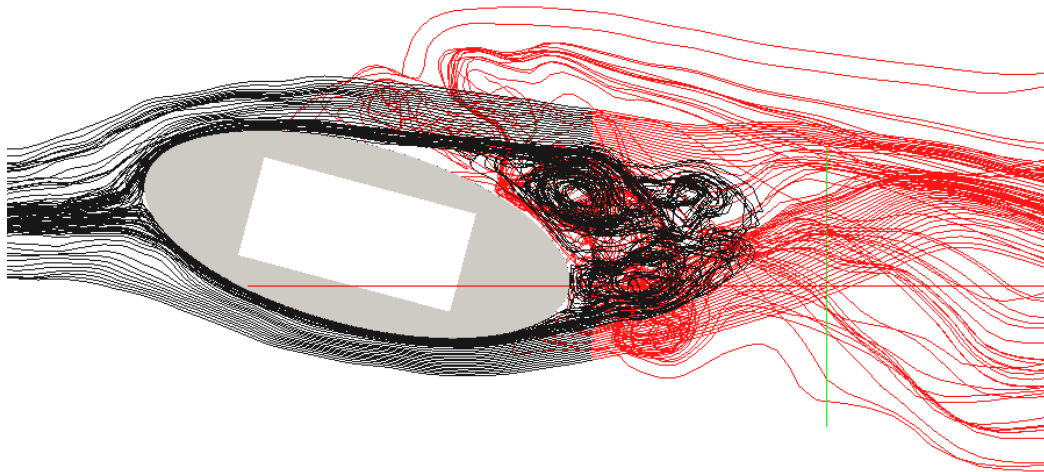
Figure 9   Example of flow around a pier visualised by streamlines initialised downstream the pier at a depth of 14m calculated using the CFD modeling system OpenFoam. Black lines are tracking backwards, red lines are tracking forward. Current angle at 0 degree (run No 1) is shown in the top view and 15 degrees (run No 11) in the bottom view.

The detailed 3-dimensional computational fluid dynamic (CFD) tools are most accurate modelling tools in studying the near field behaviour of the buoyant jet/plumes in ambient environment. The high levels of sediment concentration in the overflow and disposal plumes indicates significant dynamic and occupancy interactions in between the two phases (water, sediment), which then requires a multiphase two-way coupled solution. The application of the so-called "Boussinesq " approximation which approximates the presence of the dispersing phase only to that of change in gravitational force on the flow, is insufficient. Including the flow displacement due to the sediment fall velocity and the forces due to the transient gradients in the density and the momentum transfers due to the falling sediments are necessary for detailed calculations of the processes involved in the near field behaviour of the plumes.

The CFD model developed, evaluated and used in Saremi (2014) to study the nearfield behaviour of the overflow plumes is based on the multiphase mixture method introduced by Ishii (2006). The model uses the Large Eddy Simulation (LES) approach to resolve the turbulent eddies and solves the equations of conservation of mass and momentum for the mixture as a whole. The model was used to evaluate the effect of governing parameters on overflow plumes nearfield behaviour. In Figure 10 three snapshots of different stages (entrainment, collapse and density current over the bed) from the CFD model results simulating a material release experiment has been shown. The model is capable of resolving the dynamics of the dumping process and can be used in further investigations of various mechanisms involved in plumes evolution. See Figure 10.

Figure 10   CFD simulations of sediment dumping into stagnant ambient (Saremi, 2014)

3   Numerical tools for aquaculture site selection and environmental impact assessment (DHI)

Numerical tools are an important part of MERMAID which supports most of the work packages. As part of WP 5 hydrodynamic models coupled with ecological models have been developed to support the WP 4 and WP 7. These tools a described in present technical report.

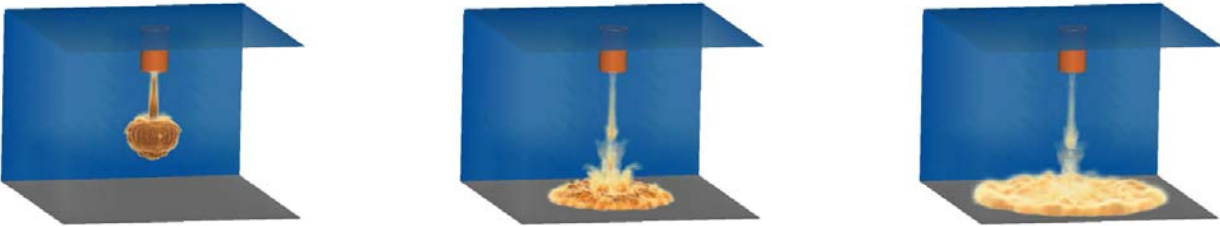Along with information on coastal infrastructures, bathymetry and presence of conflicting activities detailed knowledge of hydrodynamic conditions is fundamental for proper selection of site for sustainable and cost-efficient aquaculture. High wave exposure and prevailing strong currents will exclude most aquaculture activities due to high stress on equipment and cultured species, as will extended periods with stagnant waters because of high risks for reduced availability of oxygen in feed aquaculture and nutrients (food) in non-feed aquaculture. On the other hand, consistent (intermediate) current speeds in near-seabed and surface waters would tend to disperse particulate waste thereby preventing oxygen deficiency below aquaculture sites and disperse dissolved waste to low concentrations that the pelagic ecosystem can absorb the additional nutrients.

The MIKE-3-FM HD has been applied as the core tool used by DHI to facilitate siting of aquaculture farms and to assess the residual environmental impacts of aquaculture farm activities.

The MIKE-3 group of models is dynamic time-dependent 3-dimensional baroclinic models for free surface flows. The mathematical foundation of the models are the Reynolds-averaged Navier-Stoke's equations in three dimensions, including the effects of turbulence and variable density, together with conservation equations for mass, heat and salt, an equation of state for the density, a turbulence module and a heat exchange module. The equations are solved on either a Cartesian grid by means of the finite difference techniques (MIKE-3) or the equations are solved on an unstructured (flexible) mesh by means of finite volume/finite element techniques (MIKE 3-FM). The hydrodynamic models provide full 3-D model representation of the water levels, flows, salinity, temperature and density within the modeling domain.

The hydrodynamic model applied for location of optimal sites for macro algae production in the Inner Danish Waters (IDW), for quantifying risks for disease transmission between fish farm areas and for Environmental Impacts Assessment (EIA) of fish farms and fish farms combined with mussels farms is based on DHIs Water Forecast services for the and the Baltic Sea. The model named MIKE-3-HD-dkbs has been calibration and validated for 2010. Below is given a summary of the model.

3.1.1   Hydrodynamic model (MIKE-3-HD-dkbs)
The model mesh applied in the HD-dkbs model is shown in Figure 11 and in Figure 12 a section of the model mesh and bathymetry covering the inner Danish Waters is shown.
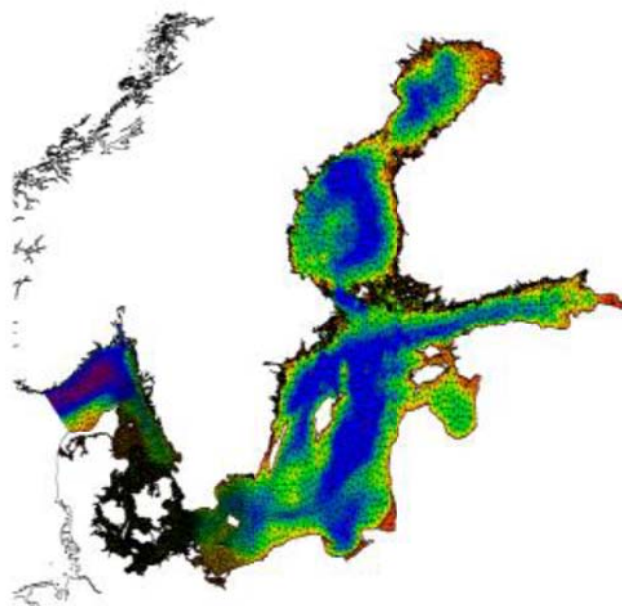
Figure 11   Model mesh of the hydro-dynamic model, MIKE-3-HDdkbs, covering the inner Danish Waters and the Baltic Sea. Colours indicate depth intervals, - shallow as red/green and deep as blue.
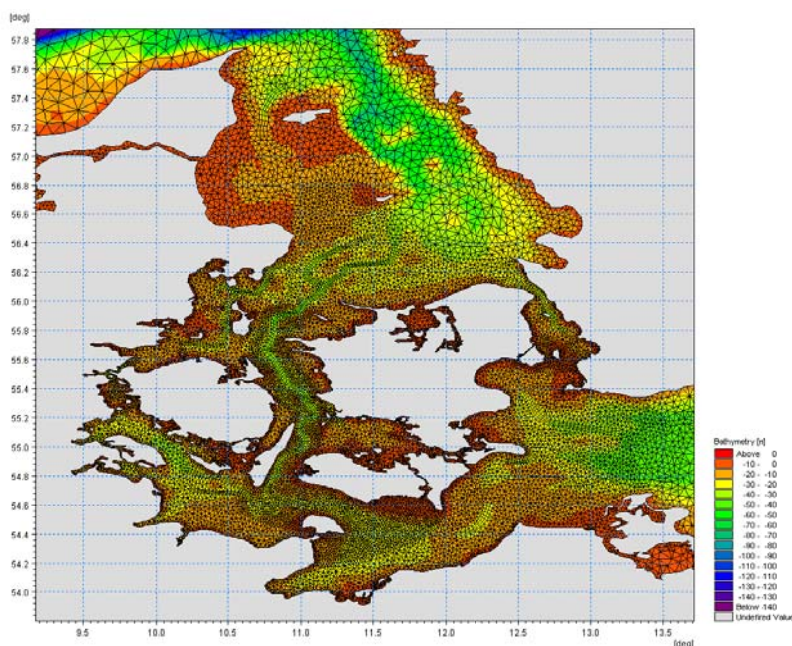
Figure 12.   Section of the computational mesh for the hydrodynamic model covering the inner Danish waters. Colors indicate depth intervals in meters.

The mesh has a resolution ranging from 500-1000 m in the Fehmarn belt area, to 1.0-2.5 km in western Baltic and Belt Sea, to 2-6 km in Kattegat and west of Bornholm, to 5-12 km in Skagerrak, and finally to 5-20 km in Baltic Sea east of Bornholm. In areas of specific interests such as in fish farm areas the horizontal resolution is increased resolving individual cages, see Figure 13.

The vertical domain is a combined sigma-z domain with the upper 10 m of the water column represented by 10 sigma-layers and the remaining water column represented by a number of z-layers depending on the local water depth. The adopted vertical resolution allows for the main part of the western Baltic Sea and the Belt Sea including Fehmarnbelt to be resolved entirely by 1 m layers.
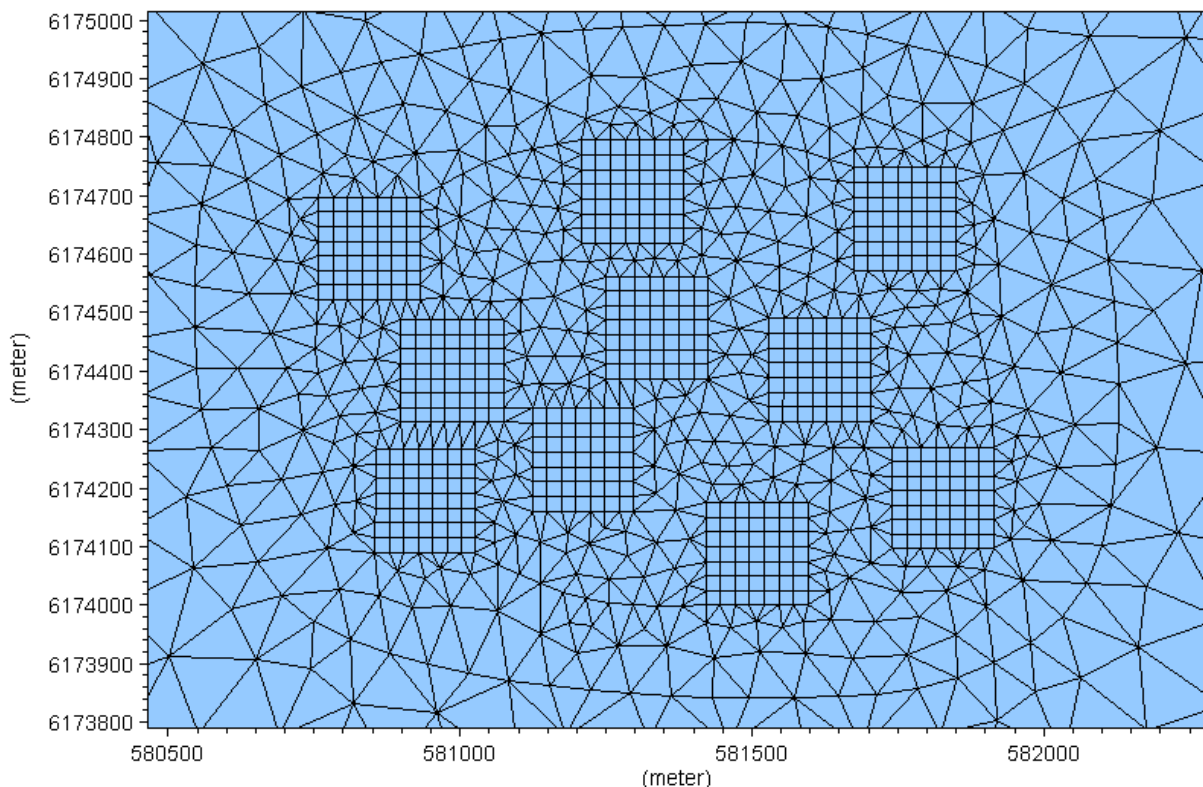
Figure 13   Section of the computational mesh for a fish farm area consisting of 10 large cages.

Meteorological input data (wind, air temperature, air pressure, clearness and precipitation) is provided by StormGeo (Norway) or DMI (Denmark).

Boundary data for the Skagerrak model boundary including water level, current, salinity and temperature are provided by DHIs larger operational forecast models: - water level and current from the Hydrostatic North Sea-Baltic Sea operational model and temperature and salinity are provided by the so-called BANSAI operational model.

In order to account for the freshwater runoff within the model domain, the hydrodynamic model includes 82 model sources. These sources represent the total freshwater input to the model domain.

Data is based on combination of modelled and climatological data from SMHIs HBV runoff model and from the data sources applied for the Danish NOVANA modeling program.

The model is calibrated by comparing simulated and measured time series of water level, water temperature and salinity at various locations (typically 10-15 stations) within the model domain.

3.1.2 MIKE-3-HD to estimate vertical advection of nutrients across pycnocline

Areas high potential for cultivation of macroalgae in the upper brackish water was identified by extracting modelled vertical currents speeds across the pycnocline located between 12 and 14 m in the Kattegat and the Great Belt. Calculated accumulated (positive) vertical velocity from 1st April through September where nutrient concentrations in surface waters is low and primary production is limited by nitrogen is shown in Figure 14, and the number of days where upwelling occurs is shown in Fig. 5. Areas with the largest accumulated upwelling (> 1.0 E3.0 m) during the nutrient-poor period occurs Langeland Belt (LB), Great Belt (GB), east of Samsø (SA) and east of Fornæs (FN). In these areas 7-10 m/d of bottom water is introduced into surface water on average.
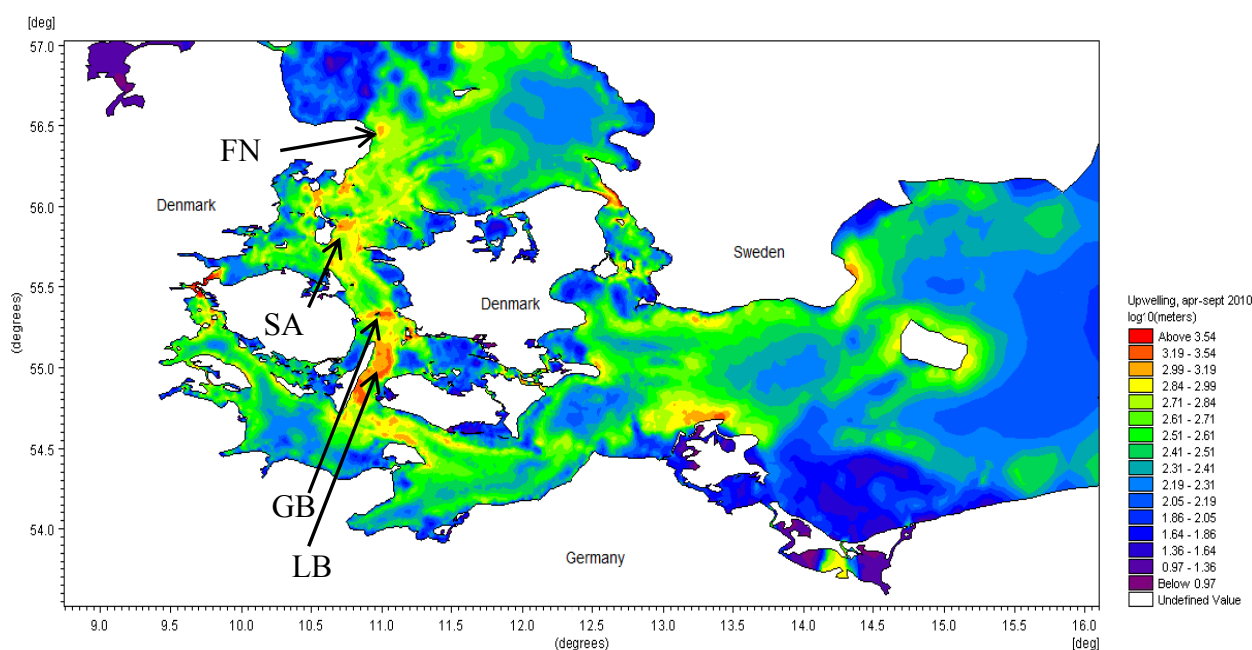
Figure 14   Accumulated positive vertical current velocities in 12 m depth for the period 1-4-2010 to 30-9-2010 for the Inner Danish Waters and the western Baltic Sea. The scale is in log10.. For areas with water depth less than 12 meters values represent positive current velocities from the bottom layer to the above layer of the model. Arrows have been inserted where upwelling is most intense (see text).

The areas identified by upwelling using the MIKE-3-FM are known from monitoring data on pelagic primary production to be highly production and thus consistent with model results.

3.1.3 MIKE-3-HD-EcoLab to estimate Hydrodynamic connectivity between fish farm sites

Waterborne transmission of fish diseases between fish farms is a potential threat for marine fish production. In order to minimize the risk of waterborne transmission of fish diseases between production sites it is important, prior to the location of new sites, to ensure that the sites have no or only little "connectivity" with other existing or planned production sites. To that end the connectivity between 35 proposed fish farm sites were quantified using "ecological" equation solver Ecolab that runs under the MIKE-3-HD.

The risk of waterborne transmission between individual fish farm was analyzed based on hydro-dynamic modelling predicting the water current in time and space, and transport (~advection-dispersion) and 1st order decay modeling describing the dissolution and transport of dissolved or suspended disease "agents" (e.g. vira , bacteria or parasite). The relative transmission risk between sites can be analyzed based on these model results: 1) Disease dispersal maps – for visual pairwise comparison of transmission risk between production sites; 2) Similarity index – a statistical method for identifying those productions sites with least (or most) risk of waterborne transmission

The disease transmission modelling was carried out using the ECO Lab module for MIKE 3 FM. The ECOLab module is an add-module for simulating the reactive transport of dissolved or suspended substances in water represented by the computational nodes (~water volumes) in the MIKE-3FM model. ECOLab is designed as an open equation solver for full customization and specification of model algorithms and variable definitions.

The disease transmission was modelled as simple 1st order decay in combination with advection dispersion processes. In order to propose most likely first order decay constants for model simulations two common fish diseases were selected, *VHS* and *Furunculosis* respectively based on available literature.

The model was setup including 35 state variables, each state variable a specific source from each of the proposed fish production sites, see Figure 15.
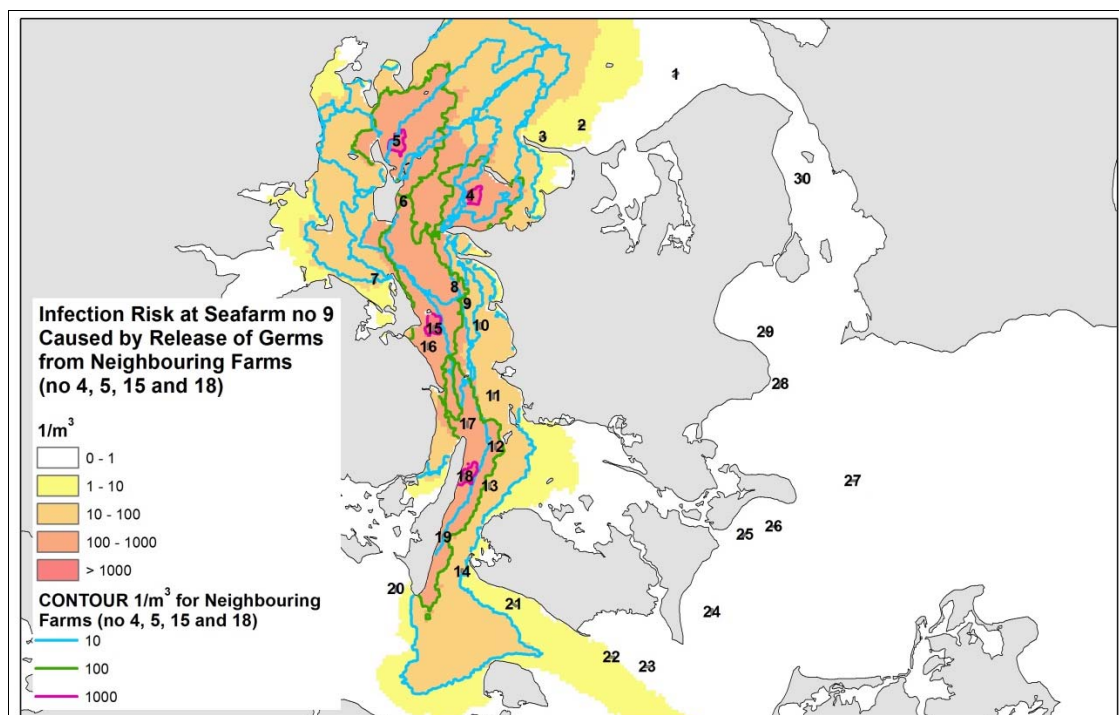
Figure 15 Disease transmission map for production site no. 9. Source was strength 106 units per second from farms neighbouring farm no. 9 (4, 5, 15, 18). First order decay constant of 0.5 per day. Yellow-red colour legend indicates simulated Maximum concentrations registered during the 3 month simulation period June – August 2005 in the upper part of the water column. Blue colours indicate depth curves of 10, 15 and 20 meters. Grey area represents land territories

3.1.4 MIKE-21-HD Screening tool to quantify dilution rates of dissolved waste from fish farms

Medicine and biocides used in finfish aquaculture to treat infected fish and as antifouling agents on nets must not exceed EU EQS outside the farm area. As an initial screening approach current speeds and dilution rates calculated based on models can provide information on where to and not to plan future fish farms. Such information can be presented in GIS formats which allow integration with other information and thus be used in marine spatial planning process.

Dilution rates in Inner Danish Waters, Western Baltic Sea and in the coastal waters of Skagerrak and the North Sea was quantified using a calibrated 2-dimensional hydrodynamic model (MIKE 21 HD) characterised by fine resolution (50x 50 m) in shallow waters gradually increasing to 1000 x 1000 m in the deeper parts of the model area (Figure 16). Being 2-dimensional the model averages current speed over depth. Hence, at larger depth (i.e. > 20 m) current speeds in surface waters will be underestimated as speed will be lower and the current direction often opposite in the saline bottom waters compared to surface waters.
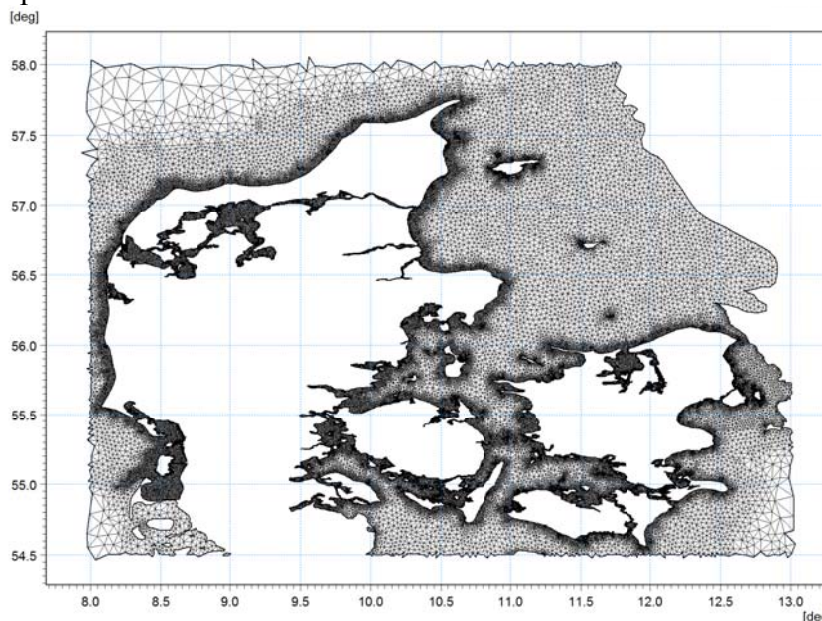
Figure 16 Model area and spatial (horizontal) resolution of MIKE 21-HD used to screen potential aquaculture sites according to dilution of dissolved waste (medicine and biocides)

The model was executed for the year 2005 and forced by meteorology, run-off, and water level, salinity and temperature at the boundaries. The model provided water level, current speed and direction in every model cell, see Figure 16.

For every model cell and at every stored time step (1 h) dilution rate was estimated as a near-field study by adding a tracer in fixed concentration and calculate tracer concentration 1000 m downstream of the release point (i.e. the fish farm) assuming default values of momentum dispersion coefficients. In order to take account of the underestimated currents speeds at larger depths we assumed that tracer concentration in surface waters (0-10 m) was representative of the real dilution. Yearly values of dilution can subsequently be calculated for each model cell as medians, averages or any percentile.

In the model area the dilution rates varied between 1,000 and 10,000 with the highest rates in Femarn Belt, the Great Belt, in the North Sea and the coastal parts of the Skagerrak (Figure 17). The lowest dilution rates were found in shallow bays, in fjords and in the Southern Little Belt.

Intuitively, all other things being equal fish farmers would select production areas where current speed is rather high and consistent to avoid periods of stagnant waters and increased risks for high temperatures and low oxygen in cages. In accordance, the newest and largest fish farm in Danish waters is located in the Great Belt where current speeds and dilutions are high.
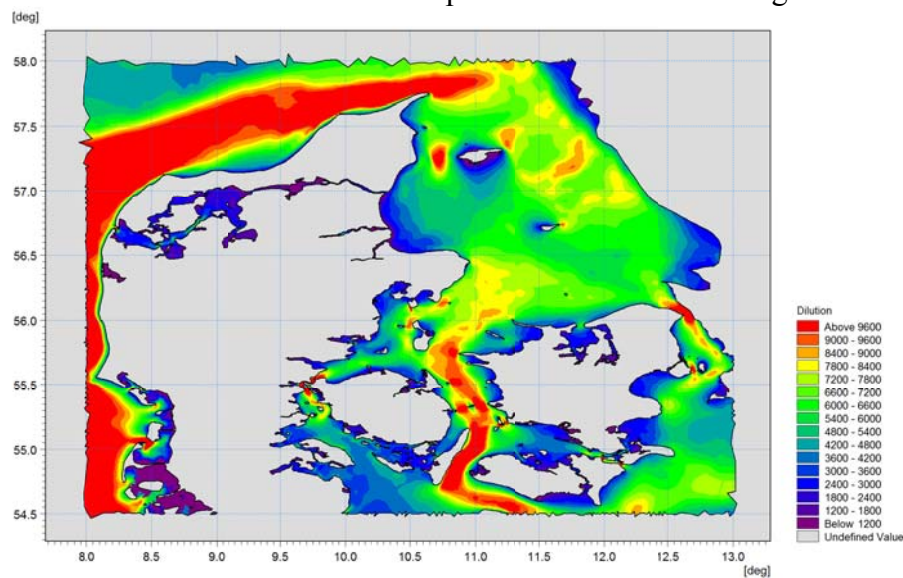
Figure 17 Dilution rate in surface waters (0-10 m) in inner Danish waters and the coastal parts of the North Sea and Skagerrak.

3.1.5 **MIKE-3-HD Lagrange-Eulerian model tool to estimate Environmental Impact Assessment of aquaculture farms at high resolution**

Along with release of medicine and biocides, the organic load of sediments and eutrophication effects resulting from release of nutrients are considered as the main environmental impacts of feed-aquaculture. For almost a decade DHI has applied coupled hydrodynamic and bio-geochemical models to estimate impacts from fish and mussel farming, including benthic effects (oxygen and sulphides in sediments and near-bed waters), phytoplankton growth and biomass accumulation, transparency in water column, growth of benthic vegetation. Using a strict Eulerean (i.e. biomass approach) spatial resolution of deposition below cages has suffered somewhat although mass conservation had been maintained. During Mermaid, the model capability has been improved by seamless combining Lagrange (agent-based modelling of deposition of faeces) and Eulerian (biomass) approaches.

A conceptual diagram of the aquaculture spill model is shown in Figure 18. The model consists of a composite of Lagrangian and Eulerian representations of the spill and fate of organic carbon from fish cages. Lagrangian particles representing feed waste and fecal particles simulate the initial spread and sedimentation of organic C from fish cages onto the sea bed. Once simulated current shear stress is below a critical threshold particles will settle and particle masses will become translated into an Eulerian state variable representing the upper layer of the sediment.

In the Eulerian model the sediment is described by 2 sediment layers that interact with the water column through erosion, re-suspension and re-deposition. The second sediment layer is included to enable consolidation of deposited material over time. Mineralization of organic carbon and the resulting oxygen consumption are simulated as part of the Eulerian model. Oxygen consumption from mineralization of "Lagrangian carbon" is also included in the mass balance equation for dissolved oxygen. The individual processes are described in more detail below.

The model was developed using a development version of the ecological modelling software ECO Lab providing full access through an open solver environment for equation development, implementation and execution on top of DHI's MIKE 3 FM. The combined ECO Lab – ABM Lab supports full integration of Eulerian and Lagrangian representations in a user-friendly environment.
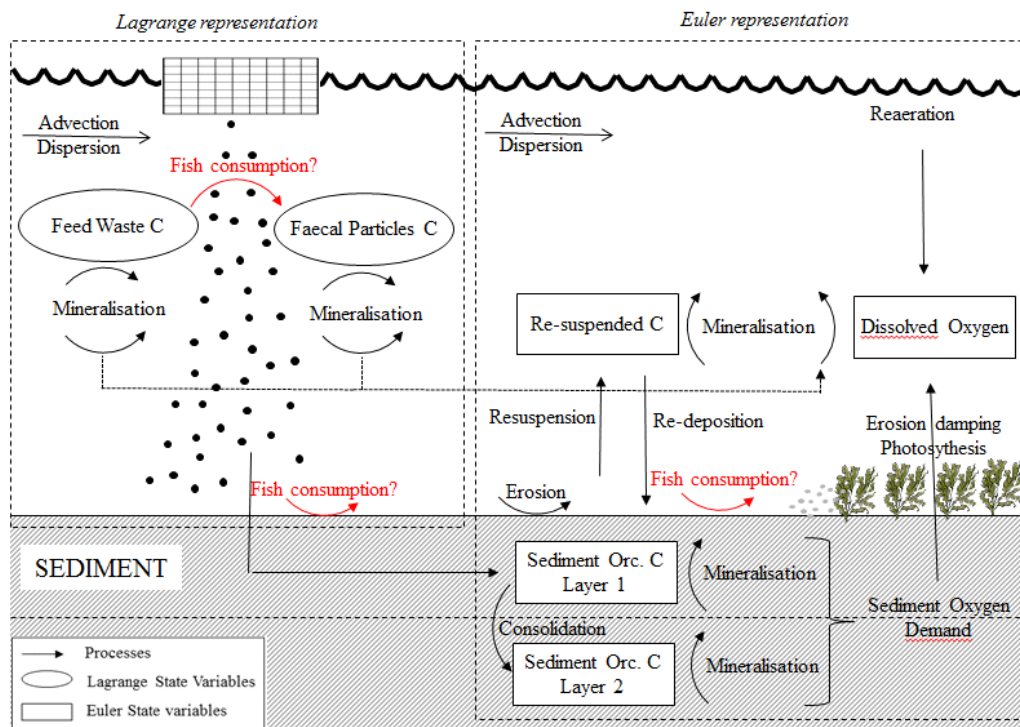
Figure 18   Conceptual diagram of the Aquaculture module as implemented in ECO Lab.

4   Use of ESA Earth Online (EO) products in MERMAID

The chapter describes how satellite data from ESA is used in MERMAID. An introduction to the data can be found at https://earth.esa.int/web/guest/home'. Earth Online will be referred to as "EO" in the following sections.

4.1   EO products description

Mediterranean Sea site
Product name: Earth Observation products over Northern Adriatic sea
Site: Mediterranean Sea
Sea name: Northern Adriatic
Product format: NetCDF
Product processing level: 3 - Binned Data Products at 1/100 or 1/30 degrees spatial resolution

North Sea site
Product name: Earth Observation products over North sea
Site: North Sea
Sea name: Wadden
Product format: NetCDF
Product processing level: 3 - Binned Data Products at 1/100 or 1/30 degrees spatial resolution

4.2   EO dataset generation workflow

In Figure 19 are reported the main processing steps for the generation and storage of Earth Observation products.
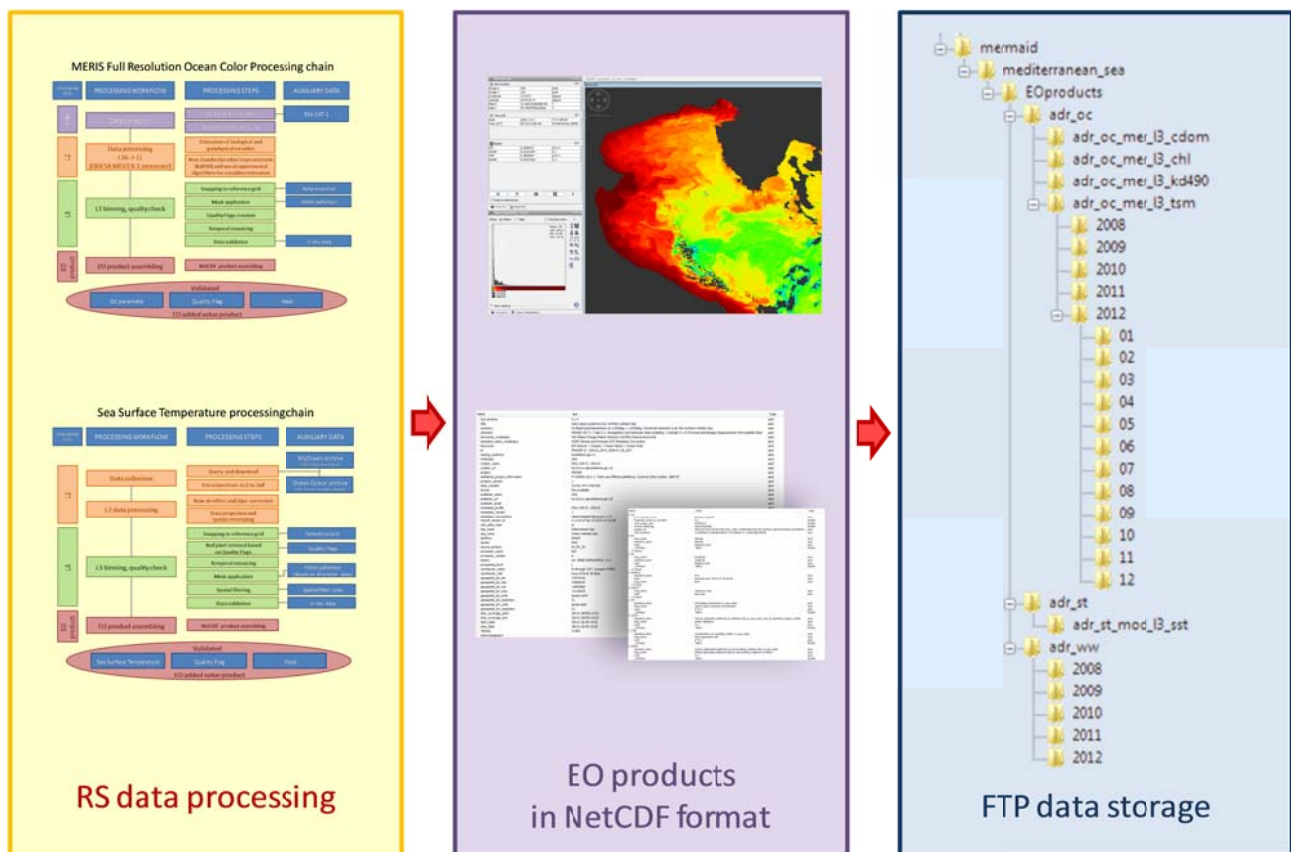
Figure 19: Earth observation dataset generation workflow.

4.3 CF-Convention Compliance

Content of all the produced NetCDF file has been checked using CF-Convention Compliance Checker for NetCDF Format (Source: http://puma.nerc.ac.uk/cgi-bin/cf-checker.pl). This form allows to check that the contents of a NetCDF file comply with the Climate and Forecasts (CF) Metadata Convention. Datasets have been successfully checked for CF-1.6 (version 1.6).

4.4 Ocean Color family product

This section describes the Ocean Color family products derived from Remote Sensing data.
List of products, spatial and temporal extent and resolution are reported in each dedicated subsection.

4.4.1 Ocean Color family product description

Optical oceanography aim to operate accurate estimation concentrations of the water constituents from optical measurements. Absorption and scattering properties of sea water are described by its inherent optical properties, or IOPs. IOPs are properties of the medium, describing its absorption and scattering properties. Apparent optical properties (AOPs) describe the bulk optical properties of water bodies, giving useful information about the types and concentrations of the water constituents from measurements of the light field. AOPs are those properties that depend both on the the IOPs

and on the directional structure of the radiance distribution, and that display enough regular features and stability to be useful descriptors of a water body (Mobley, 2010).

Based on the optical properties, waters can be classified in two main classes: Case2 waters, vertically mixed coastal waters dominated either by suspended inorganic sedimentary material or biogenic particulate material, and Case1 waters, influenced by biogenic materials only.

Depending on the concentrations of the constituents, the water changes its color from blue to green to light brown. Different bands from optical multispectral sensors are used to estimate surface concentration of photosynthetic pigment chlorophyll-a, yellow substance and suspended inorganic sedimentary particles. Algorithms are applied to derive the concentrations of the three different groups of substances in Case2 waters from the water-leaving radiance, after an atmospheric correction is performed (Doerffer, 2009).

The propagation of downwelling irradiance at specific wavelengths from surface to a depth in sea water is governed by the diffuse attenuation coefficient, Kd(λ). Kd(λ) is an apparent optical property (Preisendorfer, 1976), so it varies to some extent with solar zenith angle, sky and surface conditions, and depth. The estimation of Kd(490) (Kd at λ = 490 nm) is based on empirical relationships involving the blue-to-green ratio of water-leaving radiance (Lee et a., 2005).

Ocean Color family products have been produced using a processing chain specifically created to process optical data from MERIS, named MPOC (MERIS Processing Ocean Color). The processing chain (Figure 20) is divided in three steps: 1) the generation of L2 standard and experimental OC products, 2) generation of fully processed L2 OC products, 3) creation of L3 gridded OC products (Filipponi et al., 2014).

Final products have been estimated from data collected by MERIS optical sensor onboard ENVISAT satellite. MERIS Full Resolution data at processing level L1b have been requested to ESA with a CAT-1 agreement (Category-1 Project, n. 7963). A processing chain for parameter estimation has been built in order to produce accurate and validated spatial maps for the study site (Mediterranean Sea site, North Sea site). The L2 data are estimated from L1B products, after eliminating pixels affected by cloud coverage, sun glint or other abnormalities. After this operation an atmospheric correction algorithm is applied to subtract the atmospheric scattering components from the total radiance and thus derive the geophysical products. Standard MEGS 8.1 processor has been implemented for the computation of Kd490 parameter, which it is not included in standard MERIS L2 products. The use of experimental algorithms, based on Neural Network computational models, has been experimented for testing their possible improvements in the estimation of biological and geophysical parameters.

The L3 data are derived by binning the L2 by means of BEAM Level 3 Binning Operator, based on the NASA SeaWiFS binning algorithm as described in Campbell et al. (1995). The binning processes allowed to distribute the contributions of Level 2 pixels in satellite coordinates to a fixed Level 3 grid using a geographic reference system.

Processing chain for the 1/30 degrees spatial resolution was implemented with a spatial filtering on L3 products, in order to remove data noise due to both reprojection artifacts and spectral signal to noise ratio which is higher in MERIS Full Resolution products.

Ocean Color products have been validated using in situ data collected by moored buoys or during cruise campaigns.

Each single observation of every Ocean Color EO product is stored in a separate NetCDF file, which contains a bit mask layer indicating valid and not valid pixel (no data values).

Moreover a quality_check layer (l3_qc) in bit format is supplied, containing information for each single pixel about both acquired image quality (bit 3,4, and 5) and algorithm accuracy on the quantitative estimate value (bit 2).

Mask layer can have the following values:
0 valid
1 not_valid

l3_qc layer can have the following values:
bit0: not valid
bit1: land
bit2: low accuracy
bit3: very good
bit4: medium
bit5: poor

4.4.2 **Ocean Color family product processing chain**

This subsection reports the processing chain designed for processing the Ocean Color family products from MERIS data.

Two processing chains have been developed in order to generate Ocean Color family products from MERIS data at two different spatial resolutions, 1/100 degrees and 1/30 degrees.
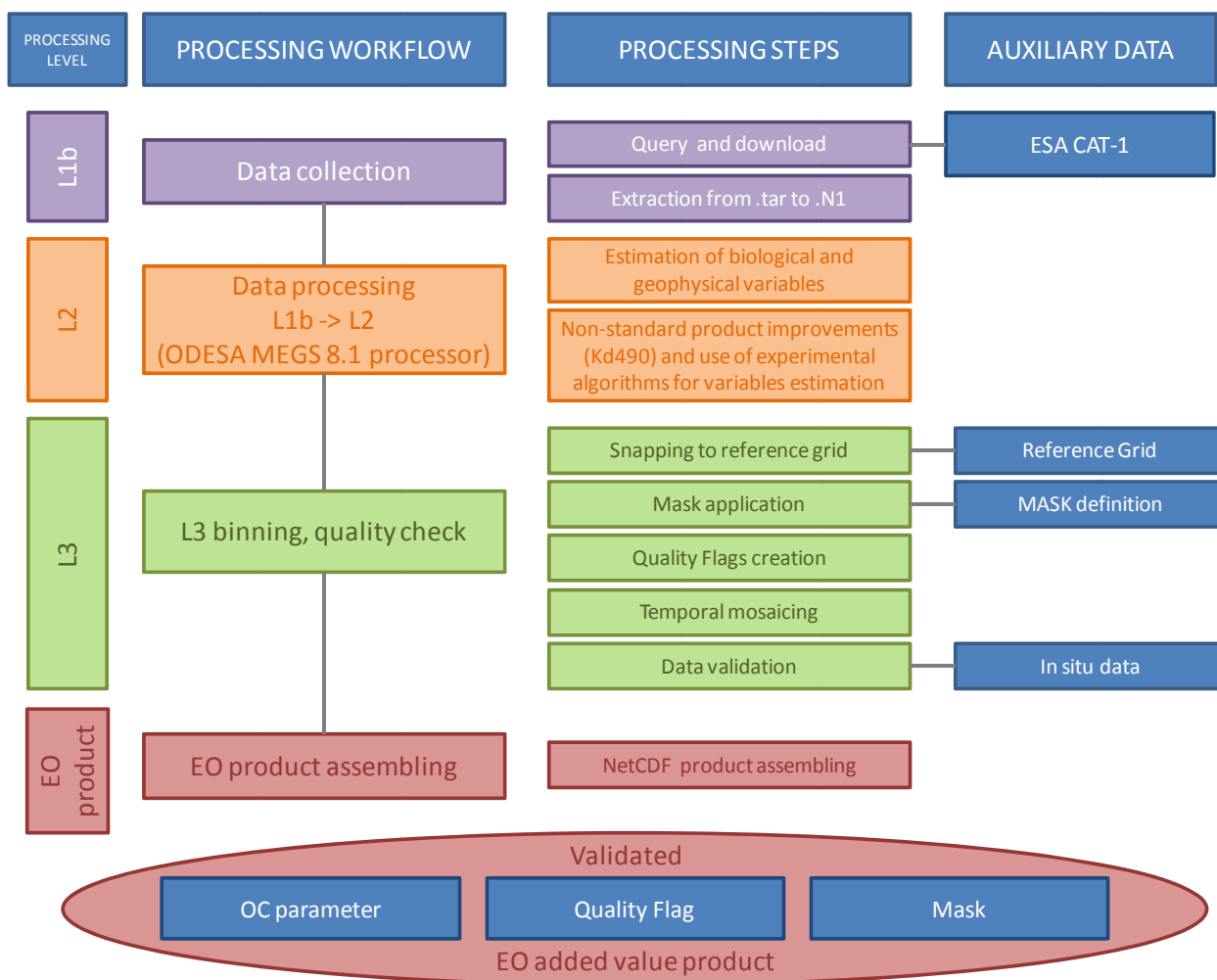
Figure 20: MERIS Ocean Color processing chain to generate EO products at 1/100 degrees spatial resolution
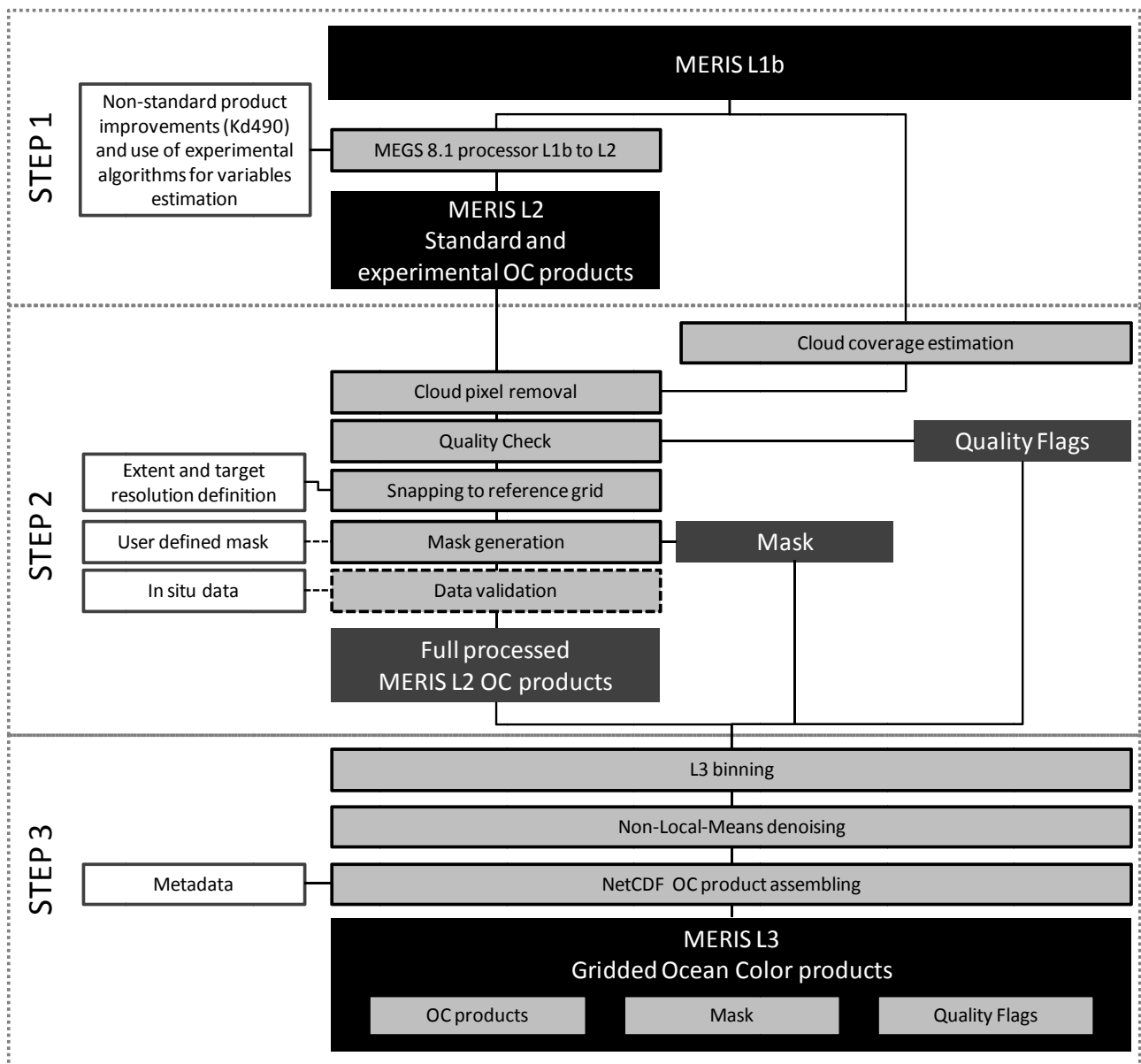
Figure 21: MERIS Ocean Color processing chain to generate EO products at 1/30 degrees spatial resolution

4.4.3 **Ocean Color family product list**

This subsection reports a list of the standard name of the Ocean Color family products, conforming to the NetCDF CF Metadata Convention.

Chl: chlorophyll_concentration_in_sea_water
CDOM: volume_absorption_coefficient_of_radiative_flux_in_sea_water_due_to_dissolved_organic_matter
TSM: concentration_of_suspended_matter_in_sea_water
Kd490: volume_attenuation_coefficient_of_downwelling_radiative_flux_in_sea_water

4.4.4 **Spatial extent and resolution**

Mediterranean Sea site

Coordinate Reference System: WGS84, EPSG:4326.
Spatial extent North: 45.9958344, South: 42.9974217, West: 11.9965566, East: 16.0110979.
Horizontal spatial resolution: 0.0083289239556 degrees; 0.003002526704222 degrees.

North Sea site
Coordinate Reference System: WGS84, EPSG:4326.
Spatial extent North: 57.1017031, South: 49.3692621, West: -3.8017031, East: 9.6874890.
Horizontal spatial resolution: 0.0034063616767525673 degrees.

4.4.5 Temporal extent and resolution

Mediterranean Sea site
Time coverage: 19/06/2002 – 02/04/2012
Time resolution: Variable, dependent on data availability and cloud coverage.
Number of observation dates: 764
Reference time: seconds since 1970-01-01 00:00:00

North Sea site
Time coverage: 15/01/2007 – 05/04/2012
Time resolution: Variable, dependent on data availability and cloud coverage.
Number of observation dates: 134
Reference time: seconds since 1970-01-01 00:00:00

4.4.6 Global attributes

This subsection reports an example of global attributes for Ocean Color family product stored in the NetCDF file.

Name	Value	Type
Conventions	CF-1.4	ascii
title	Ocean Colour products over northern Adriatic Sea	ascii
summary	Daily Biophysical parameters at 1/100deg. x 1/100deg. horizontal resolution over the northern Adriatic Sea	ascii
comment	MERMAID WP 5 > Task 5.1: Atmospheric and metocean data modelling > Subtask 5.1.5: Physical and biological measurements from satellite data	ascii
keywords_vocabulary	NASA Global Change Master Directory (GCMD) Science Keywords	ascii
standard_name_vocabulary	NetCDF Climate and Forecast (CF) Metadata Convention	ascii
keywords	Earth Science > Oceans > Ocean Optics > Ocean Color	ascii
id	ISPRA/DIP II - CRA15_2014_2008-01-26_OCP	ascii
naming_authority	isprambiente.gov.it	ascii
institution	ISPRA	ascii
creator_name	ISPRA / DIP II - CRA15	ascii
creator_url	http://www.isprambiente.gov.it/	ascii
project	MERMAID	ascii
additional_project_information	FP7-OCEAN.2011-1. Multi-use offshore platforms. Contract (GA) number: 288710	ascii
product_version	1.0	ascii
date_created	2014-02-14T17:56:40Z	ascii
license	freely available	ascii
publisher_name	ISPRA	ascii
publisher_url	http://www.isprambiente.gov.it/	ascii
publisher_email		ascii
metadata_profile	ISPRA / DIP II - CRA15	ascii
metadata_version	1.0	float64
metadata_conventions	Unidata Dataset Discovery v1.0	ascii
netcdf_version_id	4.3.1-rc2 of Jan 23 2014 17:12:28	ascii
cdm_data_type	grid	ascii
site_name	Mediterranean Sea	ascii
sea_name	Northern Adriatic Sea	ascii
platform	ENVISAT	ascii
sensor	MERIS	ascii
source_product	MER_FR_1P	ascii
processor_name	MEGS	ascii
processor_version	8.1	float64
history	orbit: 30880 ISPRA/MPOC v1.0	ascii
processing_level	L3	ascii
contributor_name	ESA through CAT-1 project #7963	ascii
contributor_role	Source of level 1B data	ascii
geospatial_lat_min	42.9974218	float64
geospatial_lat_max	45.9958344	float64
geospatial_lon_min	11.9965566	float64
geospatial_lon_max	16.0110979	float64
geospatial_lat_units	degrees north	ascii
geospatial_lat_resolution	0.01	float64
geospatial_lon_units	degrees east	ascii
geospatial_lon_resolution	0.01	float64
time_coverage_start	2008-01-26T09:14:32	ascii
time_coverage_end	2008-01-26T09:14:32	ascii
start_date	2008-01-26 09:14:32	ascii
stop_date	2008-01-26 09:14:32	ascii
TileSize	360:482	ascii
acknowledgment		ascii

Figure 22: Global attributes for Ocean Color product family stored in NetCDF file

4.4.7 Variable attributes

This subsection reports an example of variable attributes for Ocean Color family product stored in the NetCDF file.

Name	Value	Type
⊟ crs		
grid_mapping_name	latitude_longitude	ascii
longitude_of_prime_meridian	0.0	float64
semi_major_axis	6378137.0	float64
inverse_flattening	298.257223563	float64
spatial_ref	GEOGCS["WGS 84",DATUM["WGS_1984",SPHEROID["WGS 84",6378137,298.257223563,AUTHORITY...	ascii
GeoTransform	11.9965566 0.0083289239556 0 45.9958344 0 -0.0083289239556	ascii
⊟ lat		
long_name	latitude	ascii
standard_name	latitude	ascii
units	degrees_north	ascii
_FillValue	-999.0	float32
⊞ Values		
⊟ lon		
long_name	longitude	ascii
standard_name	longitude	ascii
units	degrees_east	ascii
_FillValue	-999.0	float32
⊞ Values		
⊟ obstime		
standard_name	time	ascii
units	seconds since 1970-01-01 00:00:00	ascii
long_name	time	ascii
⊞ Values		
⊟ reftime		
long_name	reference_time	ascii
units	text_time	ascii
⊞ Values		
⊟ Chl		
standard_name	chlorophyll_concentration_in_sea_water	ascii
long_name	case2 waters chlorophyll concentration	ascii
units	g*m-3	ascii
_FillValue	-999.0	float32
⊟ CDOM		
standard_name	volume_absorption_coefficient_of_radiative_flux_in_sea_water_due_to_dissolved_organic_matter	ascii
long_name	yellow substance	ascii
units	m-1	ascii
_FillValue	-999.0	float32
⊟ TSM		
standard_name	concentration_of_suspended_matter_in_sea_water	ascii
long_name	total suspended matter	ascii
units	g*m-3	ascii
_FillValue	-999.0	float32
⊟ Kd490		
standard_name	volume_attenuation_coefficient_of_downwelling_radiative_flux_in_sea_water	ascii
long_name	Diffuse attenuation coefficient (KD) for downwelling irradiance at 490nm	ascii
units	m-1	ascii
_FillValue	-999.0	float32

Figure 23: Variable attributes for Ocean Color product family stored in NetCDF file

⊟ Chl
standard_name	chlorophyll_concentration_in_sea_water	ascii
long_name	case2 waters chlorophyll concentration	ascii
units	g*m-3	ascii
_FillValue	-999.0	float32

⊟ mask
long_name	Mask of data	ascii
valid_range.0	0	int8
valid_range.1	1	int8
flag_values.0	0	int8
flag_values.1	1	int8
_FillValue	-1	int8
flag_meanings	valid not_valid	ascii
_Unsigned	true	ascii

⊟ l3_qc
long_name	Quality check for Level 3 oc products	ascii
_FillValue	-1	int8
valid_range.0	0	int8
valid_range.1	13	int8
flag_values.0	0	int8
flag_values.1	1	int8
flag_values.2	2	int8
flag_values.3	3	int8
flag_values.4	4	int8
flag_values.5	11	int8
flag_values.6	12	int8
flag_values.7	13	int8
flag_meanings	land very_good medium poor not_valid very_good_with_low_accuracy medium_with_low_accuracy poor_with_low_accuracy	ascii
_Unsigned	true	ascii

Figure 24: Variable attributes for Chlorophyll Ocean Color product stored in NetCDF file, together with mask and l3_qc layers
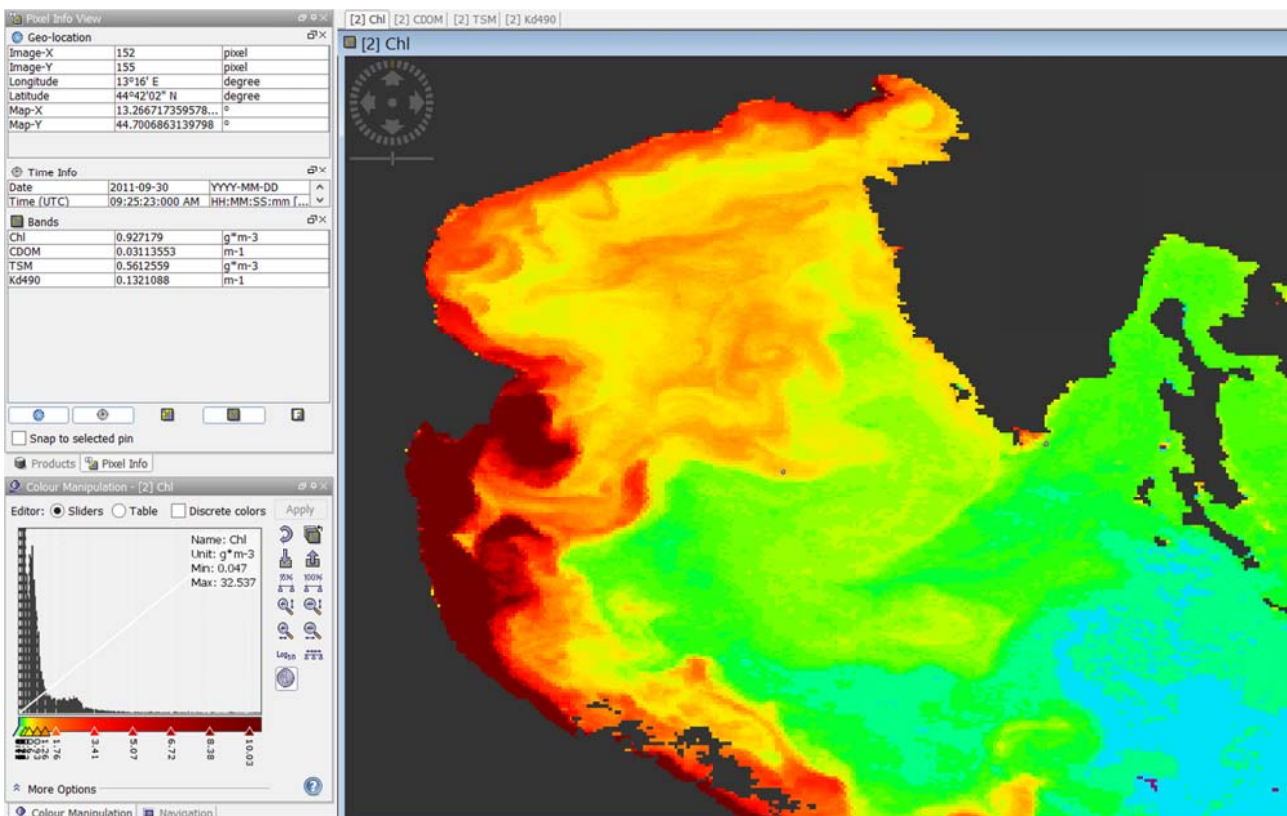

Figure 25: Example of Chl product map

4.5 Sea Temperature family product

This section describes the Sea Temperature family products derived from Remote Sensing data.
List of products, spatial and temporal extent and resolution are reported in each dedicated subsection.

4.5.1   Sea Temperature family product description

One of the most useful successful oceanographic applications from weathers and Earth Observation satellite data is the mapping of Sea Surface Temperature (SST) from infrared imagery.
Algorithms for deriving SST from RS data has been enhanced from first procedures (Anding and Kauth, 1970) to the improved optimal estimates of water surface temperature (Merchant et al., 2008). Since observation of SST from space is an important element of the global observing system for numerical weather prediction (NWP) and climate monitoring, users requirements for the accuracy of SST steadily become more demanding (Merchant et al., 2008).

Sea Surface Temperature product for the Mediterranean Sea site has been produced using a processing chain specifically created to process data from MODIS.
Final products have been estimated from data collected by MODIS optical sensor onboard Terra satellite. MODIS data at processing level L2 have been requested to OceanColor archive. A processing chain for parameter estimation has been built in order to produce accurate and validated spatial maps for the study site (Mediterranean site, Northern Adriatic sea). Standard SST product has been corrected for bow-tie effect and stripes using ENVI-IDL® with EPOC plugin. Quality check processing step using Quality Flag values has been used to remove all bad pixels. Spatial filtering has been applied in order to reduce area with low number of valid pixels.

Sea Surface Temperature product for the North Sea site has been estimated from data collected by AASTR (Advanced Along-Track Scanning Radiometer) sensors on board ENVISAT satellite. It is the most recent instruments designed primarily to measure Sea Surface Temperature, following ATSR-1 and ATSR-2 on board ERS-1 and ERS-2. AASTR L2P data have been requested to ESA using the FTP data archive through a CAT-1 agreement (Category-1 Project, n. 7963). L2P data, containing full resolution dual-view Sea Surface Temperature (SST) values, have been first filtered on the base of quality level of measurement and then reprojected and resampled by means of BEAM Level 3 Binning Operator, based on the NASA SeaWiFS binning algorithm as described in Campbell et al. (1995). The binning processes allowed to distribute the contributions of Level 2 pixels in satellite coordinates to a fixed Level 3 grid using a geographic reference system.

Each single observation of SST EO product is stored in a separate NetCDF file, which contains a bit mask layer indicating valid and not valid pixel (no data values).
Moreover a quality_check layer (l3_qc) is supplied, containing information for each single pixel about both acquired image quality (value 1) and algorithm accuracy on the quantitative estimate value (value 6).

Mask layer can have the following values:
0 valid
1 not_valid

l3_qc layer can have the following values:
0 valid
6 interpolated
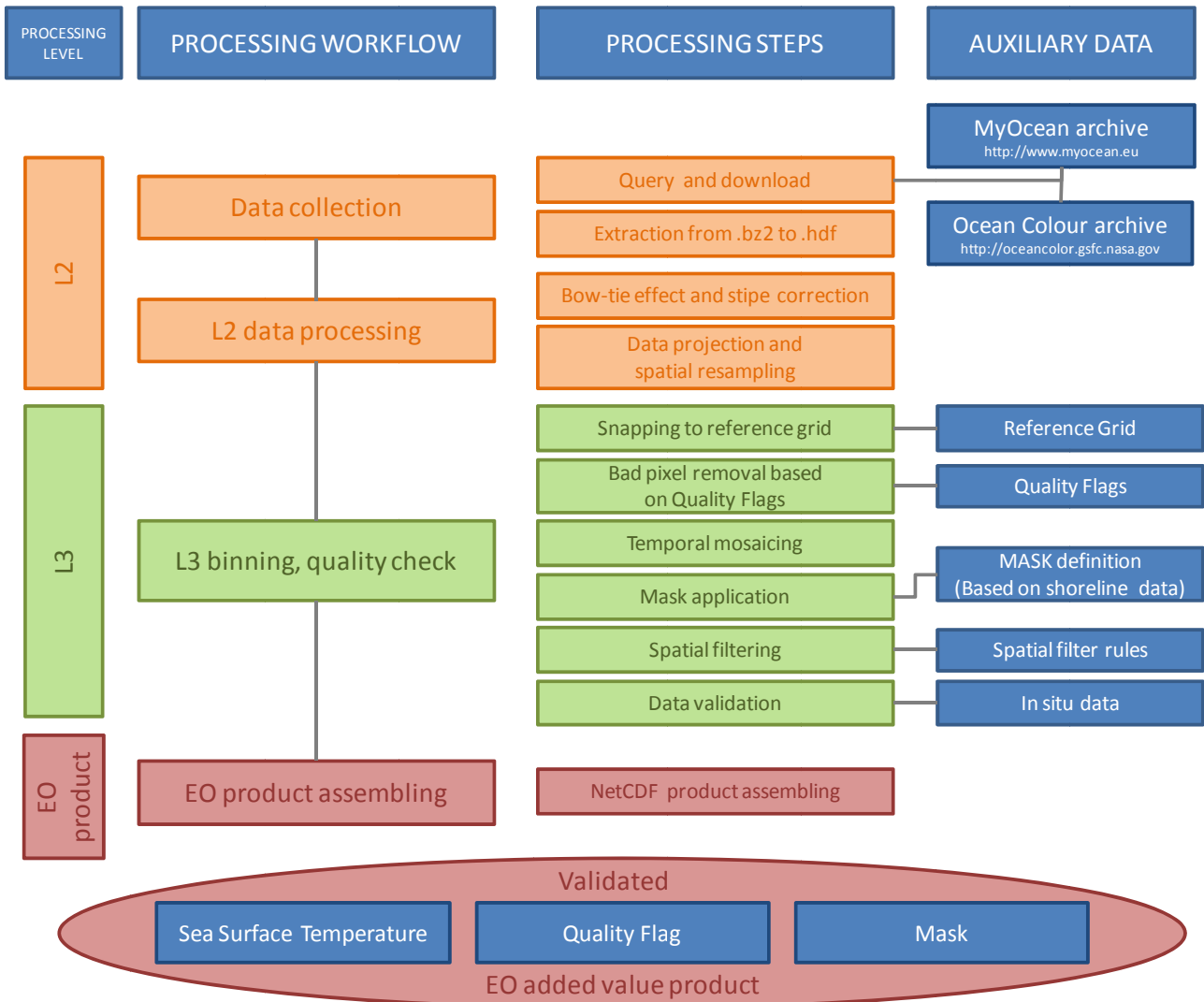
Figure 26: Sea Surface Temperature processing chain

4.5.2 **Sea Temperature family product list**

This subsection reports the standard name of the Sea Surface Temperature product, conforming to the NetCDF CF Metadata Convention.
SST: sea_surface_temperature

4.5.3 **Spatial extent and resolution**

Mediterranean Sea site
Coordinate Reference System: WGS84, EPSG:4326.
Spatial extent North: 45.9958344, South: 42.9974217, West: 11.9965566, East: 16.0110979.
Horizontal spatial resolution: 0.0083289239556 degrees.

North Sea site
Coordinate Reference System: WGS84, EPSG:4326.
Spatial extent North: 57.1017031, South: 49.3692621, West: -3.8017031, East: 9.6874890.
Horizontal spatial resolution: 0.0083289239556 degrees.

4.5.4 Temporal extent and resolution

Mediterranean Sea site
Time coverage: 10/05/2003 – 02/05/2013
Time resolution: Daily, there can be missing data because of cloud coverage.
Number of observation dates: 3646
Reference time: seconds since 1970-01-01 00:00:00

North Sea site
Time coverage: 01/01/2007 – 07/04/2012
Time resolution: Daily, there can be missing data because of cloud coverage.
Number of observation dates: 1621
Reference time: seconds since 1970-01-01 00:00:00

4.6 Ocean surface wind field family product

This section describes the Ocean surface wind field family product derived from Remote Sensing data.

List of products, spatial and temporal extent and resolution are reported in each dedicated subsection.

4.6.1 Ocean surface wind field family product description

Ocean surface wind field can be measured at high resolution (up to 300 m) from remote sensing Synthetic Aperture Radar (SAR).

Wind blowing on the ocean surface generates surface roughness generally aligned with the wind direction. Satellite radar backscatter has the capability of measuring sea surface roughness, which is related to the wind speed and direction. The estimation of wind field (speed and direction) is achieved with the inversion of geophysical model function, operated by different retrieval algorithms like CMOD (Hersbach et al., 2007) and XMOD (Ren et al., 2012) for different sensor characteristics (C-band and X-band SAR imagery).

Wind field products have been collected from SOPRANO service, developed by CLS (Collecte Localisation Satellites). Envisat ASAR Wide Swath Mode data VV polarized have been processed using SAR2WNF software v.3.0.0. Scattering model used to estimate wind field from NRCS (Normalized Radar Cross Section) is CMOD-IFR2 (Quilfen et al., 1998) for NRCS developed by for VV-polarized C-band scatterometry, using a priori wind direction from ECMWF 33 hours wind forecast at 0.25 degrees resolution.

Example of use of SAR wind fields as forcing in wave downscaling is described in Gutiérrez et al. (in press).

4.6.2 Ocean surface wind field family product list

This subsection reports the standard name of the Ocean surface wind field product, conforming to the NetCDF CF Metadata Convention.

wind_speed: wind_speed
wind_from_direction: wind_from_direction
un: eastward_wind
vn: northward_wind

4.6.3 Spatial extent and resolution

Mediterranean Sea site
Coordinate Reference System: WGS84, EPSG:4326.
Spatial extent North: 45.9958344, South: 42.9974217, West: 11.9965566, East: 16.0110979.
Horizontal spatial resolution: 0.0083289239556 degrees.

4.6.4 Temporal extent and resolution

Mediterranean Sea site
Time coverage: 04/12/2011 – 08/04/2012
Time resolution: Variable, dependent on data availability.

Number of observation dates: 15
Reference time: seconds since 1970-01-01 00:00:00

4.6.5 Variable attributes

This subsection reports an example of variable attributes for Ocean surface wind field family product stored in the NetCDF file.

Name	Value	Type
Conventions	CF-1.6	ascii
title	Ocean surface wind field over northern Adriatic Sea	ascii
summary	Wind speed and direction at 1/100deg. x 1/100deg. horizontal resolution over the northern Adriatic Sea	ascii
comment	MERMAID WP 5 > Task 5.1: Atmospheric and metocean data modelling > Subtask 5.1.5: Physical and biological measurements ...	ascii
keywords_vocabulary	NASA Global Change Master Directory (GCMD) Science Keywords	ascii
standard_name_vocabulary	NetCDF Climate and Forecast (CF) Metadata Convention	ascii
keywords	Earth Science > Oceans > Ocean Winds > Surface Winds	ascii
id	ISPRA/DIP II - CRA15_2014_wind_product_2012-02-02	ascii
naming_authority	isprambiente.gov.it	ascii
institution	ISPRA	ascii
creator_name	ISPRA / DIP II - CRA15	ascii
creator_url	http://www.isprambiente.gov.it/	ascii
project	MERMAID	ascii
additional_project_information	FP7-OCEAN.2011-1. Multi-use offshore platforms. Contract (GA) number: 288710	ascii
product_version	1.0	ascii
date_created	2014-05-28T16:41:29Z	ascii
license	freely available	ascii
publisher_name		ascii
publisher_url		ascii
publisher_email		ascii
metadata_profile	ISPRA / DIP II - CRA15	ascii
metadata_version	1.0	float64
metadata_conventions	Unidata Dataset Discovery v1.0	ascii
netcdf_version_id	4.3.1-rc2 of Aug 20 2013 18:05:19	ascii
cdm_data_type	grid	ascii
site_name	Mediterranean Sea	ascii
sea_name	Northern Adriatic Sea	ascii
platform	Envisat	ascii
sensor	ASAR	ascii
source_product	WSM_1P	ascii
processor_name	SAR2WNF V3.0.0	ascii
processor_version	7.0	float64
history	branche rev1102eor [r7750#0] 20110928T11:30:41Z - Scattering Model: CM0D_IFR2(BC) NN - ISPRA processing chain	ascii
processing_level	L3	ascii
contributor_name	CLS - Collecte Localisation Satellites	ascii
contributor_role	Source of level 3 data	ascii
geospatial_lat_min	42.9974218	float64
geospatial_lat_max	45.9958344	float64
geospatial_lon_min	11.9965566	float64
geospatial_lon_max	16.0110979	float64
geospatial_lat_units	degrees north	ascii
geospatial_lat_resolution	0.01	float64
geospatial_lon_units	degrees east	ascii
geospatial_lon_resolution	0.01	float64
time_coverage_start	2012-02-02T20:59:29	ascii
time_coverage_end	2012-02-02T20:59:29	ascii
start_date	2012-02-02 20:59:29	ascii
stop_date	2012-02-02 20:59:29	ascii
TileSize	360:482	ascii
acknowledgment	CLS SOPRANO	ascii

Figure 27: Global attributes for Ocean surface wind field product family stored in NetCDF file

Name	Value	Type
⊞ lat		
⊞ lon		
⊟ time		
long_name	time	ascii
standard_name	time	ascii
units	seconds since 1970-01-01 00:00:00	ascii
calendar	standard	ascii
axis	T	ascii
⊞ Values		
⊟ wind_speed		
units	m s-1	ascii
standard_name	wind_speed	ascii
long_name	Wind speed	ascii
_FillValue	-999.0	float32
⊟ wind_direction		
units	degrees	ascii
standard_name	wind_from_direction	ascii
long_name	Wind direction (meteorological convention)	ascii
_FillValue	-999.0	float32
⊟ un		
units	m s-1	ascii
standard_name	eastward_wind	ascii
long_name	Eastward wind velocity	ascii
_FillValue	-999.0	float32
coordinates	time lat lon	ascii
⊟ vn		
units	m s-1	ascii
standard_name	northward_wind	ascii
long_name	Northward wind velocity	ascii
_FillValue	-999.0	float32
coordinates	time lat lon	ascii

Figure 28: Variable attributes for Ocean surface wind field product family stored in NetCDF file

4.7 EO products data storage

This section describes the structure and convention used for data storage in FTP server.

4.7.1 EO products folder structure

This subsection describes the structure of the folder where the EO products are stored.

Data are stored in NetCDF format in a FTP server, the folder structure containing data files is divided in the different study sites. Inside each site folder, the subfolder "EOproducts" contains all the products created from RS data, divided in the three families described in chapter 2 of this document.

Subfolder of "EOproducts" are named using a string with constant length (number of characters = 5) which describe the site sea and EO product family. In the example the Northern Adriatic sea ("adr") is reported, folder names are:

adr_oc: Northern Adriatic sea Ocean Color product family

adr_st: Northern Adriatic sea Sea Temperature product family

adr_ww: Northern Adriatic sea Wind Wave product family

Data contained in the three product family folders are ordered on the basis of temporal coverage.

EO products have been processed for each single observation, and stored in subfolder following a temporal order. Monthly mean data are available only for Sea Temperature products. Ocean Color family products are stored in separate NetCDF file, one for each single product (chl, cdom, tsm, kd490).
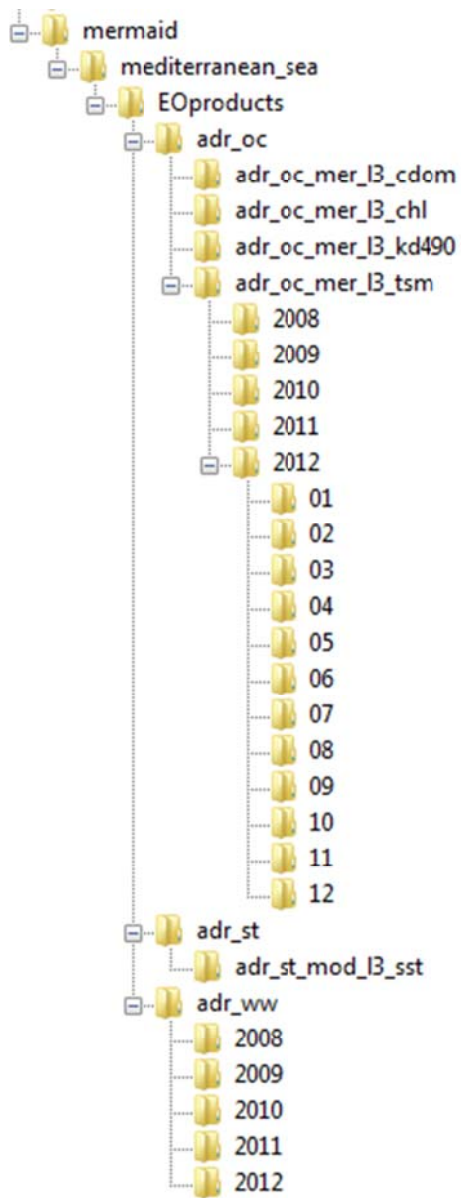
Figure 29: FTP storage structure

4.7.2 **EO products file name convention**

This subsection describes the structure of the file name of the EO products.
File name is a string with constant length, for this reason some product names are followed by one or more underscore symbol "_".

File name format:
YYYYMMDD_HHMMSS_TTT_CC_RRR_lX_PPPPP_vZZ.FF

where:
YYYY=year of acquisition
MM=month of acquisition
DD=day of acquisition
HH=hour of acquisition
MM=minute of acquisition
SS=second of acquisition
TTT=Site (adr=Northern Adriatic sea, wad=Wadden Sea)
CC=EO product family ("oc"=Ocean Color, "st"=Sea Temperature, "ww"=Wind Wave)
RRR=Acquisition Source (mer=MERIS, mod=MODIS, asa=ASAR, ers=ERS, tsx=TerraSAR-X, rs2=RADARSAT2, csk=Cosmo-SkyMED, myo=MyOcean)
l=Processing Level
X=Processing Level number (0,1,2,3,4)
PPPPP=product ("chl__"=Chlorophyll-a, "cdom_"=Colored Dissolved Organic Matter, "tsm__"=Total Suspended Matter, "kd490"= diffuse attenuation coefficient for downwelling irradiance at 490nm, "sst__"=Sea Surface Temperature, "wind_"="wind field", "wave_"=waves)
v=product version
ZZ=version number
FF=file format (nc=NetCDF, tif=GeoTIFF)

File name example is showed here:
20080126_091432_adr_oc_mer_l3_chl___v01.nc

4.8 EO products validation

This subsection describes the validation procedure and results of the EO products.

Earth Observation products have been validated for the Mediterrenean Sea site using in situ data collected from buoys, cruise campaigns and water quality monitoring acquisitions.

Validated products are SST, wind, Chl and TSM, while in situ data for CDOM and Kd490 were not available for spatial and temporal range of the dataset.

4.9 Ocean Color family product validation

Ocean Color products have been validated, using cruise campaigns data and water quality monitoring acquisitions, for the period 13/02/2008 – 20/12/2011.

As the measurements have not been collected at the same time of the satellite acquisitions, differences in the comparison are evident. For this reason, only qualitative comparison have been done for Chlorophyll (Chl) and Total Suspended Matter (TSM) EO products.
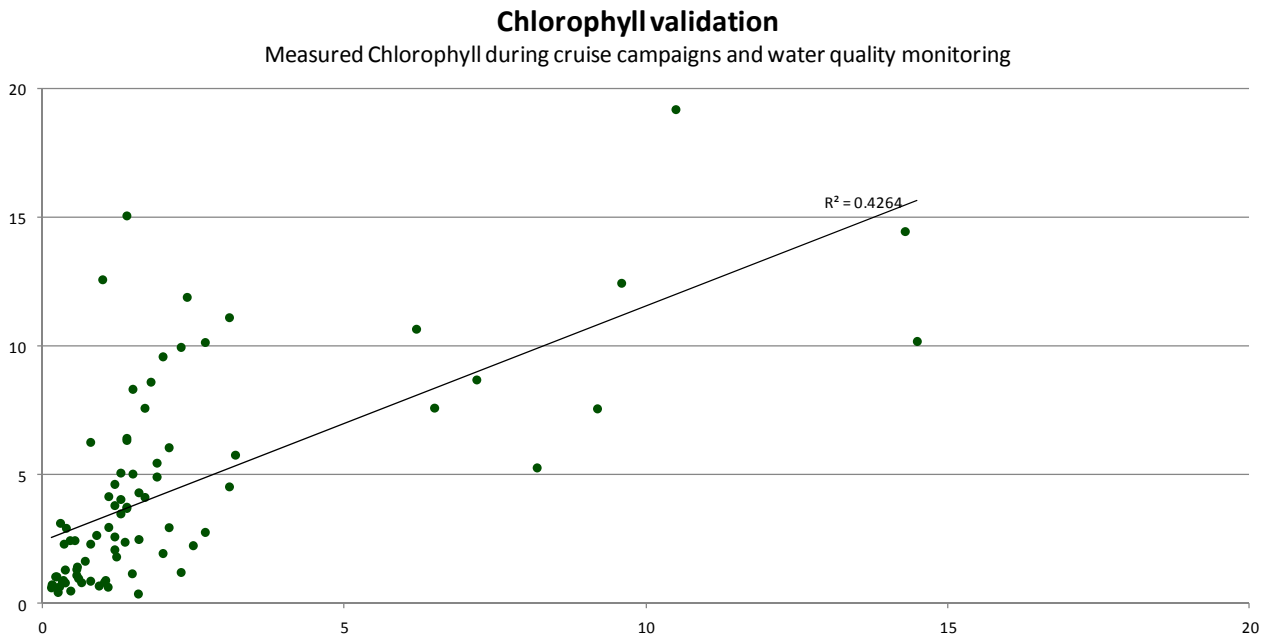

Figure 30: Comparison of measured Chlorophyll during cruise campaigns and water quality monitoring and estimated Chlorophyll from satellite data
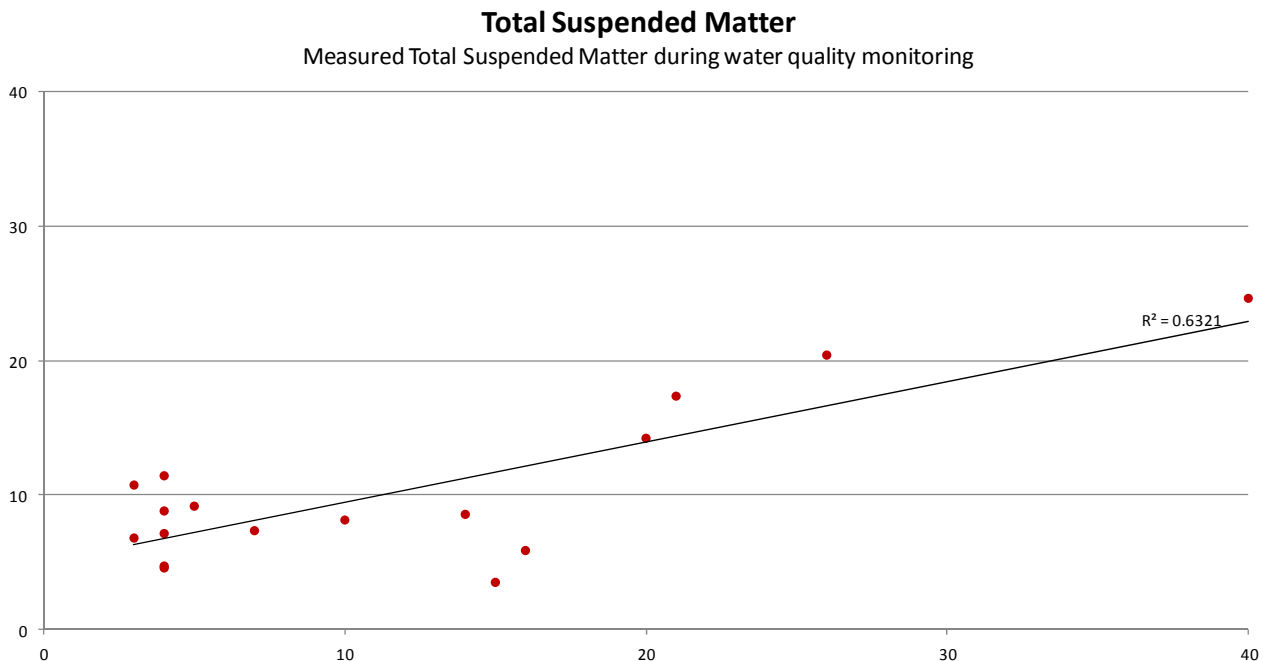
Total Suspended Matter

Measured Total Suspended Matter during water quality monitoring

Figure 31: Comparison of measured Total Suspended Matter during water quality monitoring and estimated Total Suspended Matter from satellite data

4.10 Sea Temperature family product validation

SST products have been validated, using in situ acquisition from ISPRA Venice RON buoy, for the period 01/04/2010 – 31/10/2012.

Temporal profile of SST from buoy acquisition has been extracted from multitemporal dataset by means of spatial queries and plotted (Figure 32). In situ data have been superimposed in the temporal profile in order to visualize the trend of both observed and estimated data.

Scatterplot have been created to compare observed and estimated SST data, Mean Error (ME), Root Mean Square Error (RMSE) and Coefficient of determination (R2) have been calculated for the EO product.

Data comparison showed high precision of SST product estimation from RS data, statistical analysis resulted with ME: 1.00 (°C); RMSE: 1.42 (°C); R2: 0.92.
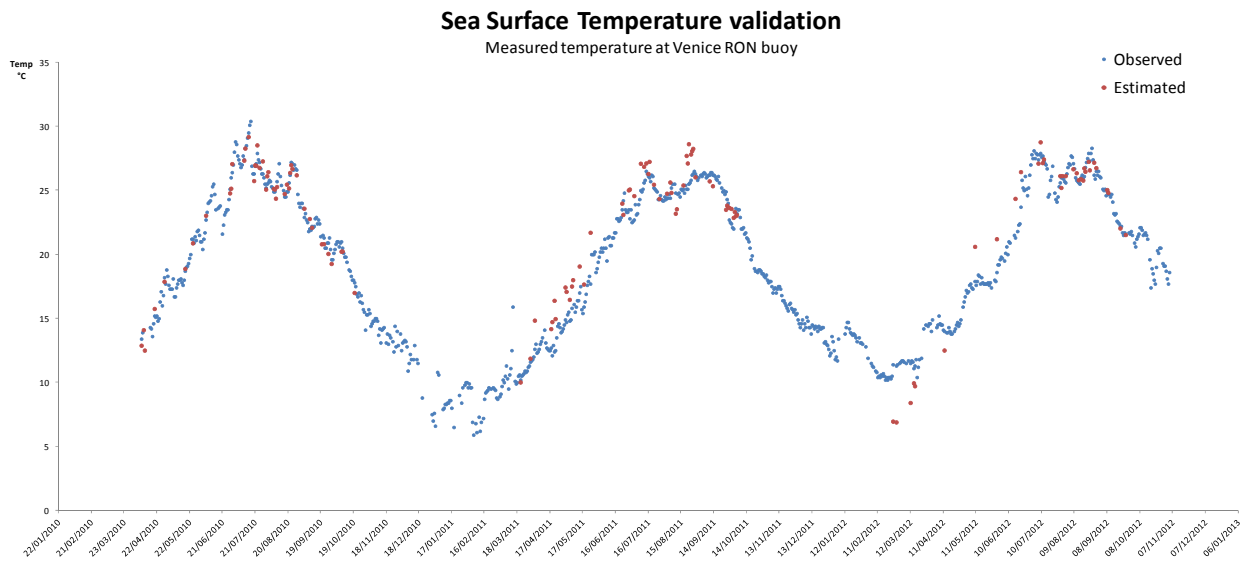
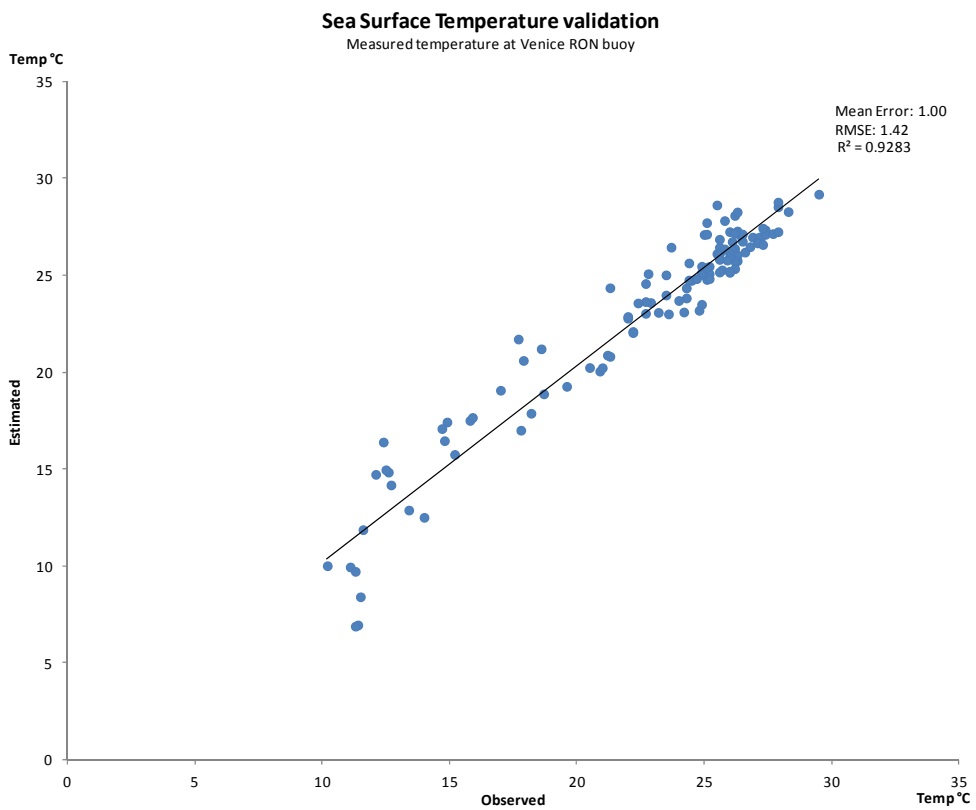*Figure 32: Time series of measured and estimated Sea Surface Temperaure*

Figure 33: Comparison of measured and estimated Sea Surface Temperature

4.11 Ocean surface wind field family product validation

Wind speed and direction estimated from SAR measurements has been compared to in situ data collected from ISPRA Venice RON buoy, CNR-ISMAR Acqua Alta Tower, GNL terminal and ARPAV buoy. Wind fields refer to the acquisitions of the period December 2011 – April for which SAR data were collected and processed for the Mediterranean Sea site.

Scatterplot have been created to compare observed and estimated wind field data, Mean Error (ME), Root Mean Square Error (RMSE) and Coefficient of determination (R2) have been calculated for both wind speed and wind direction products.

Data comparison showed very high precision of wind field products estimation from ENVISAT-ASAR data, statistical analysis resulted with ME: 1.71 (m/s); RMSE: 1.30 (m/s); R2: 0.76 for wind speed and ME: 27.87 (degrees); RMSE: 5.27 (degrees); R2: 0.92 for wind direction.
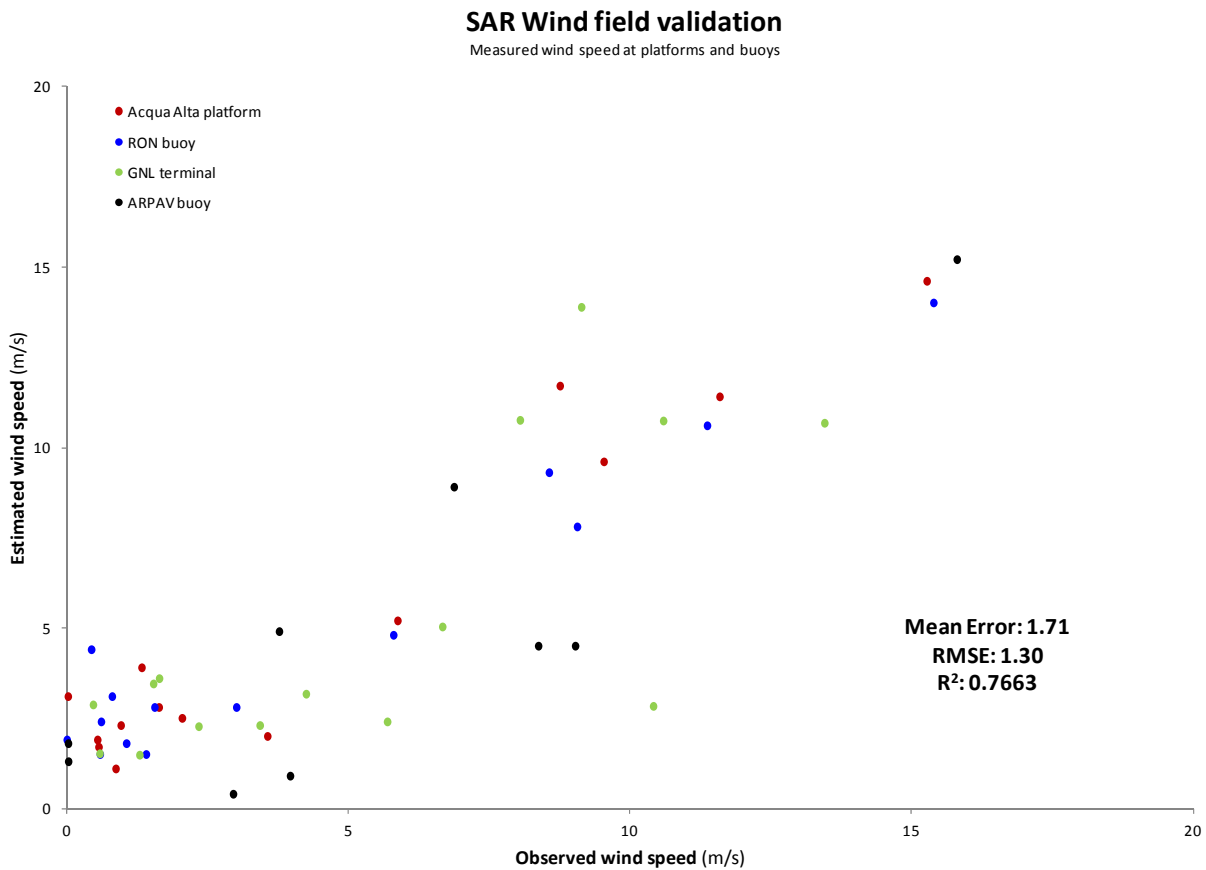

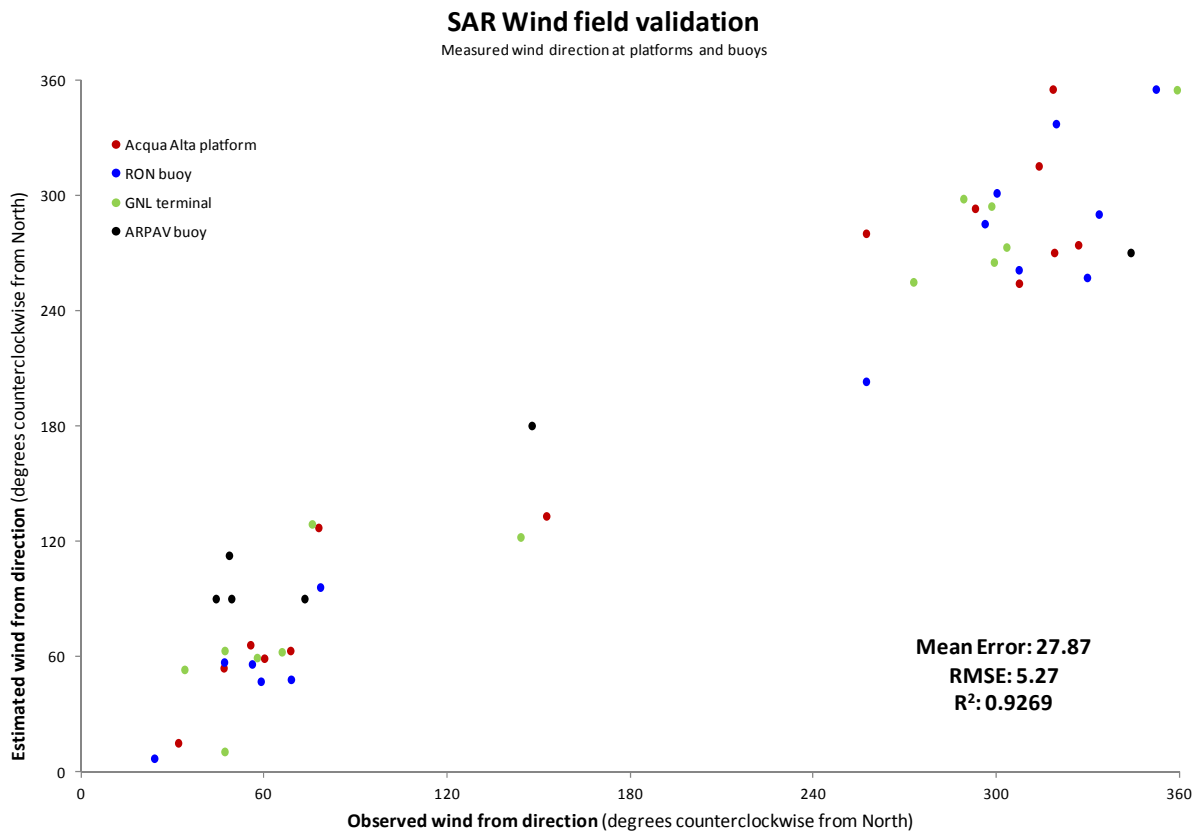
Figure 34: Comparison of measured and estimated wind speed

Figure 35: Comparison of measured and estimated wind direction

5   References

Anding D., Kauth R., 1970. Estimation of sea surface temperature from space. Remote Sensing of the Environment, vol. 1, pp. 217–220.

Augustin, L.N. 2007. Laboratory experiments and numerical modeling of wave attenuation though artificial vegetation. Coastal Engineering 88 (2014) 131-142.

Bredmose, H., & Jacobsen, N. G. (2011). Vertical wave impacts on offshore wind turbine inspection platforms. In *International Conference on Ocean, Offshore and Arctic Engineering*.

Brennan, D. (2001): The Numerical Simulation of Two-Phase Flows in Settling Tanks, *PhD Thesis*, Imperial College of Science, Technology and Medicine.

Buchholz, C.M. , Krause, G. and Buck, B., 2012. Seaweed and Man.

Buck, B. and Buchholz, C.M., 2005. Response of offshore cultivated   Laminariasaccharina to hydrodynamic forcing in the North Sea. ScienceDirect, Aquaculture 250 (2005) 674-691.

Campbell J.W., Blaisdell J.M. and Darzi M., 1995. Volume 32, Level-3 SeaWiFS Data Products: Spatial and temporal binning algorithms, in SeaWiFS Technical Report Series, NASA Technical Memorandum 104566, Vol. 32.

Dalrymple, R., Kirby, J., and Hwang, P. (1984). "Wave Diffraction Due to Areas of Energy Dissipation." J. Waterway, Port, Coastal, Ocean Eng., 110(1), 67–79.

Davis, N.N., Hahmann, A.N., Clausen, N.-E. and Žagar, M., 2014: Forecast of icing events at a wind farm in Sweden. Journal of Applied Meteorology and Climatology, 53, no. 2, pp. 262-281, 10.1175/JAMC-D-13-09.1

Dee, D.P. et al., 2011. The ERA-Interim reanalysis: configuration and performance of the data assimilation system. Quart. J. Roy. Meteorol. Soc. 137 (656), 553–597.

Dijkstra, J. T., and R. E. Uittenbogaard, 2010. "Modeling the interaction between flow and highly flexible aquatic vegetation", Water Resour. Res., 46, W12547, doi:10.1029/2010WR009246.

Doerffer R., Sørensen K., Aiken J., 2009. MERIS potential for coastal zone applications. Intenational Journal of remote sensing, 1999, vol. 20, no. 9, 1809-1818.

Draxl C, Hahmann AN, Peña A, Giebel G. 2014. Evaluating winds and vertical wind shear from WRF model forecasts using seven PBL schemes. Wind Energy 14: 39–55, doi: 10.1002/we.1555.

Feagin, R.A. et al., 2011. Short communication: Engineering properties of wetland plants with application to wave attenuation. Coastal Engineering 58 (2011) 251-255.

Filipponi F., Valentini E., Liberti L., Zucca F., Taramelli A., 2014. Generation of gridded Ocean Color products from MERIS: an efficient processing chain. IEEE GOLD REMOTE SENSING CONFERENCE 2014, Berlin 5-6 June, Proceedings. (in press)

Fuhrman, D., Dixen, M., & Jacobsen, N. G. (2010). Physically-consistent wall boundary conditions for the k-ω turbulence model. *Journal of Hydraulic Research, 48*(6), 793–800. doi:10.1080/00221686.2010.531100

Gutiérrez O.Q., Filipponi F., Valentini E., Taramelli A., Camus P., Mendez F.J., (in press). On the feasibility of the use of wind SAR to downscale waves on shallow water. Proceedings of ESA-SOLAS-EGU 2014 Earth Observation for Ocean-Atmosphere Interactions Science, Frascati (Italy) 28-31 October 2014.

Hahmann A.N., Lennard C., Argent B., Badger J., Vincent C.L., Kelly M.C., Volker P.J.H., Refslund J., 2014b. Mesoscale modeling for the wind atlas for South Africa (WASA) Project. Technical Report, DTU Wind Energy, Roskilde, Denmark

Hahmann, A.N., D. Rostkier-Edelstein, T. T. Warner, Y. Liu, F. Vandenberg, R. Babarsky, and S. P. Swerdlin, 2010: A reanalysis system for the generation of mesoscale climatographies. J. Appl. Meteor. Climatol., 49, 954-972.

Hahmann, A.N., Lange, J., Peña Diaz, A. & Hasager, C.B., 2012: The NORSEWInD numerical wind atlas for the South Baltic. DTU Wind Energy. DTU Wind Energy E, no. 0011(EN).

Hahmann, A.N., Vincent, C.L., Peña, A., Lange, J. and Hasager, C.B., 2014a: Wind climate estimation using WRF model output: method and model sensitivities over the sea. International Journal of Climatology, 10.1002/joc.4217.

Hersbach H., Stoffelen A., De Haan S., 2007. An improved C-band scatterometer ocean geophysical model function: CMOD5. Journal of Geophysical Research, vol. 112, no. C03006, pp. 1–18.

Hirt, C., & Nichols, B. (1981). Volume of fluid (VOF) method for the dynamics of free boundaries. *Journal of Computational Physics, 39*(1), 201–225. doi:10.1016/0021-9991(81)90145-5

Ishii, M. (2006). Thermo-Fluid Dynamics of Two-Phase Flow. Springer US, Boston, MA.

Jacobsen, N. G., Fuhrman, D. R., & Fredsøe, J. (2012). A wave generation toolbox for the open-source CFD library : OpenFoam. *International Journal for Numerical Methods in Fluids, 70,* 1073–1088. doi:10.1002/fld

Jasak, H., Jemcov, A., & Tukovic, Z. (2007). OpenFOAM : A C ++ Library for Complex Physics Simulations ˇ. In *International Workshop on Coupled Methods in Numerical Dynamics* (Vol. m, pp. 1–20).

Jensen, B., Christensen, E. D., & Jacobsen, N. G. (2014). Simulation of extreme events of oblique wave interaction with porous breakwater structures. In *International Conference on Coastal Engineering* (pp. 1–13).

Jensen, B., Jacobsen, N. G., & Christensen, E. D. (2014). Investigations on the porous media equations and resistance coefficients for coastal structures. *Coastal Engineering*, *84*, 56–72. doi:10.1016/j.coastaleng.2013.11.004

Larsén, X.G., Badger, J., Hahmann, A.N. & Mortensen, N.G., 2012: The selective dynamical downscaling method for extreme-wind atlases. Wind Energy, 16, pp. 1167–1182, 10.1002/we.1544.

Larsén, X.G., Ott, S., Badger, J., Hahmann, A.N. & Mann, J., 2012: Recipes for correcting the impact of effective mesoscale resolution on the estimation of extreme winds. Journal of Applied Meteorology and Climatology, 51, no. 3, pp. 521-533, 10.1175/JAMC-D-11-090.1.

Lee Z.P., Darecki M., Carder K.L., Davis C.O., Stramski D., Rhea W.J., 2005. Diffuse attenuation coefficient of downwelling irradiance: An evaluation of remote sensing methods. Journal of geophysical research, Vol. 110, C02017, doi:10.1029/2004JC002573.

Maike, P., 2014. "Evaluation of the use of surrogate Laminaria digitata in eco-hydraulic laboratory experiments. " ScienceDirect, Journal of Hydrodynamics, 2014, 26(3):374-383.

Marinelli, M., Maule, P., Hahmann, A.N., Gehrke, O., Nørgård, P.B. and Cutululis, N.A., 2014: Wind and Photovoltaic Large-Scale Regional Models for hourly production evaluation. IEEE Transactions on Sustainable Energy, 10.1109/TSTE.2014.2347591.

Mellor, G. L. and T. Yamada, 1982: Development of a turbulence closure model for geophysical fluid problems, Rev. Geophys. and Space Phys., 20, 851-875.

Mendez, F.M., Losada, I.J., 2004. An empirical model to estimate the propagation of random breaking and nonbreaking waves over vegetation fields. Coast. Eng. 51, 103–118.

Merchant C.J., Le Borgne P., Marsouin A., Roquet H., 2008. Optimal estimation of sea surface temperature from split-window observations, Remote Sensing of the Environment, 112(5), 2469-2484. doi:10.1016/j.r2007.11.011.

Mobley C., Boss E., Roesler C., 2010. Ocean Optics Web Book. http://www.oceanopticsbook.info, consulted at 15/01/2014.

OpenFoam (2014). http://openfoam.org/docs/user/

Paul, M. et al., 2013. "Geometrical and mechanical properties of four species of northern European brown macroalgae." Coastal Engineering 84 (2014) 73-80.

Paulsen, B. T., Bredmose, H., Bingham, H. B., & Jacobsen, N. G. (2014). Forcing of a bottom-mounted circular cylinder by steep regular water waves at finite depth. *Journal of Fluid Mechanics*, *755*, 1–34. doi:10.1017/jfm.2014.386

Peña A, Hahmann AN. 2012. Atmospheric stability and turbulence fluxes at Horns Rev – an intercomparison of sonic, bulk and WRF model data. Wind Energy, 15: 717–731, doi: 10.1002/we.500.

Preisendorfer R.W., 1976. Hydrologic Optics. Vol. 1, Introduction, National Technical Information Service, Springfield, Va.

Quilfen Y., Chapron B., Elfouhaily T., Katsaros K., Tournadre J., 1998. Observation of tropical cyclones by high-resolution scatterometry. Journal of Geophysical Research, vol. 103, no. C4, pp. 7767–7786.

Ren Y., Lehner S., Brusch S., Li X., He M., 2012. An algorithm for the retrieval of sea surface wind fields using X-band TerraSAR-X data. International Journal of Remote Sensing, vol. 33, no. 23, pp. 7310-7336.

Reynolds, R. W., N. A. Rayner, T. M. Smith, D. C. Stokes, and W. Q. Wang, 2012: An improved in situ and satellite SST analysis for climate. J. Climate, 15, 1609–1625.

Rusche H. Computational fluid dynamics of dispersed two-phase flows at high phase fractions. *PhD Thesis*, Impirical College of Science, Technology and Medicine, December 2002. Available at: http://powerlab.fsb.hr/-ped/kturbo/OpenFOAM/docs/HenrikRuschePhD2002.pdf.

Saremi, S. (2014). Density driven currents and deposition of fine materials (Doctoral dissertation). Technical University of Denmark, Lyngby, Denmark.

Skamarock W.C., Klemp J.B., Dudhia J., Gill D.O., Barker D.M., Duda M.G., Huang X.-Y., Wang W., Powers J.G.. 2008. A description of the advanced research WRF Version 3. Technical Report NCAR/TN–475+STR, National Center for Atmospheric Research, Boulder, CO.

Suzuki , T. et al., 2011. "Wave dissipation by vegetation with layer schematization in SWAN." Coastal Engineering 59 (2011) 64–71

Villiers, E. De (2006): The Potential of Large Eddy Simulation for the Modelling of Wall Boundary Flows, *PhD Thesis*, Imperial College of Science, Department of Mechanical Engineering.

Vincent CL, Larsén XG, Larsen SE, Sørensen P., 2012. Cross-spectra over the sea from observations and mesoscale modelling. Bound.-Layer Meteorol. 1460(2): 297–318, doi: 10.1007/s10546- 012-9754-1.

Wang, W., C. Bruyere, M. Duda, J. Dudhia, D. Gill, H-C. Lin, J. Michaelakes, S. Rizvi, and X. Zhang. WRF-ARW Version 3 Modeling System User's Guide. Mesoscale & Microscale Meteorology Division, National Center for Atmospheric Research, Boulder, USA, 2009.

Zhan Hu et al., "Laboratory study on wave dissipation by vegetation in combined current-wave flow." Coastal Engineering 88 (2014) 131-142.